International Scientific-Technical and Production Journal

The Paton WELDING JOURNAL

April 2003 # 4

English translation of the monthly «Avtomaticheskaya Svarka» (Automatic Welding) journal published in Russian since 1948

Founders: *The E.O. Paton Electric Welding Institute of the NAS of Ukraine*
International Association «Welding»

Publisher: *International Association «Welding»*

Address:
E.O. Paton Electric Welding Institute,
International Association «Welding»,
11, Bozhenko str., 03680, Kyiv, Ukraine
Tel.: (38044) 227 67 57
Fax: (38044) 268 04 86
E-mail: journal@paton.kiev.ua
http://www.nas.gov.ua/pwj

State Registration Certificate
KV 4790 of 09.01.2001

Subscriptions:
$460, 12 issues per year,
postage and packaging included.
Back issues available.

CONTENTS

EVALUATION OF CONDITION OF METAL OF WELDED PIPES OF LONG-OPERATED GAS PIPELINES

S.E. SEMYONOV[1], **A.A. RYBAKOV**[1], **L.V. GONCHARENKO**[1], **T.N. FILIPCHUK**[1], **M.N. DROGOMIRETSKY**[2] and **B.I. PEDKO**[2]
[1]E.O. Paton Electric Welding Institute, NASU, Kyiv, Ukraine
[2]GK «UKRTRANSGAS», Kyiv, Ukraine

Service properties of specimens of pipes, cut from operating gas pipeline and also from pipes of emergency stock, are investigated. The feasibility of preserving serviceability of pipe metal after the long-term service is shown. It was established that the decreased characteristics of metal strength of separate pipes as compared with rated values are not due to the effect of service loads. To provide the safe service of the old gas pipelines it is necessary to reveal and remove the metal defects and also to perform the diagnostic examinations with identification of laid-out pipes, evaluation of level of technical characteristics and stability of quality.

Key words: *gas pipeline, material, service, investigation, service properties, condition, ageing*

Some works, devoted to the evaluation of condition of operating gas and oil pipelines, show the opinion about the negative effect of long-time service on the performance of material of main pipelines.

As a result of our earlier investigations of material of oil pipelines being for a long time in service (up to 35 years) [1, 2], no significant changes were revealed in major service properties of pipe metal, that allowed us to make conclusion about the possibility to preserve the performance of metal of pipelines in the process of their long-time force loading. However, the possibility of appearance of local changes in crack resistance of metal of pipelines, due to deformation ageing, is not excluded [3, 4].

Unlike the oil pipelines the avalanche fractures are possible in gas pipelines. Consequences of the processes of material ageing can be very hazardous for the operation of gas pipelines. Therefore, it is important to preserve strength and, in particular, toughness in metal of long-operated gas pipelines.

Accumulation of data about the properties of metal of long-operated gas pipelines will make it possible to judge with a high validity of the effect of a factor of long-time loading on the pipeline material.

In this connection, the condition of metal of pipe specimens, cut from operating gas pipelines, and also from corresponding pipes of emergency stock, was investigated.

Until the 1970s the pipes from normalized and hot-rolled pipes were used in construction of gas pipelines. Pipes from advanced steels of a controllable rolling began to be used later. Terms of service of these gas pipelines do not exceed, as a rule, 20 years.

In the present work the pipe specimens corresponding to a large range of materials of gas pipelines with a long enough period of service (more than 20 years) were investigated. The study of behaviour of pipes of a controllable rolling steel in a long-time service with allowance for specific features of structure and chemical composition represents a special interest.

Seamless hot-deformed pipes of 508 mm diameter (steel of 19G type) were delivered in the 1950–1970s from the former Czechoslovakia. Unlike the welded pipes they have an increased difference in walls.

Hot-straightened pipes of 529 mm diameter of production of Iljich Zhdanov Metallurgical Works were first manufactured for the system of main oil and gas pipelines in the former USSR from sheet silicon-manganese steel 10G2SD (later 10G2S1) with a decreased (to 0.12 %) content of carbon. The use of a single-sided welding of longitudinal weld was an essential drawback of the technological process of their manufacture, though the mechanical characteristics of the parent metal and welded joint were significantly improved due to a hot straightening of pipes in heating up to the temperature of steel normalizing.

The longitudinally-welded pipes of 720 (steel 17GS) and 1220 mm (17G1S) diameters of manufacture by Chelyabinsk Pipe-Rolling Plant, and also the pipes of 1020 mm diameter (steel 17G1S) of manufacture by Novomoskovsk Pipe Plant (NPP) were the most widely spread products supplied for the construction of oil and gas pipelines. Unlike the pipes of 530–820 mm diameter, manufactured from hot-rolled steel, the pipes of 1020 and 1220 mm diameters were manufactured only from the normalized sheets.

Pipes, manufactured in Germany from the normalized sheet steel of 17G1SF type, were used for the first time in the construction of gas pipelines of 1420 mm diameter.

Before 1975 (until introducing SNiP II-45–75) the pipes were manufactured without taking into consideration several current requirements to their quality. In particular, the metal of pipes was not controlled by criteria used for evaluating the resistance to avalanche fractures. The 100 % ultrasonic control of sheet rolled metal and welded joints of pipes, obligatory in modern conditions, was not also made. After introducing requirements concerning the impact

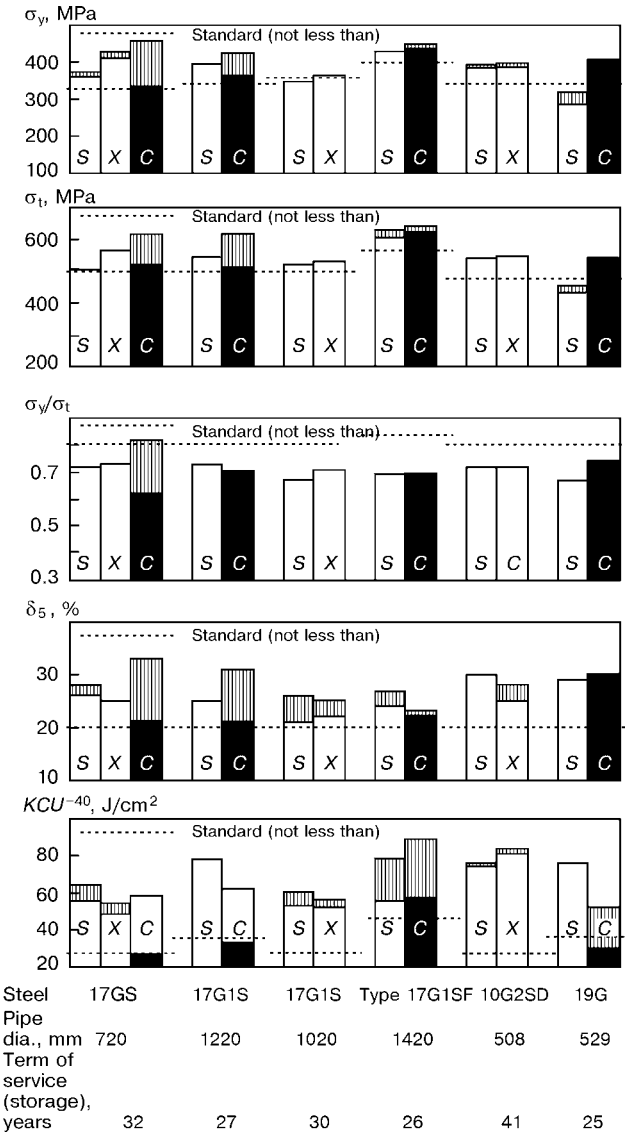

Figure 1. Mechanical properties of parent metal of pipes investigated: *S* — as-serviced pipes; *X* — emergency stock pipes; *C* — certificate data (hatched zone — region of values scattering)

strength on specimens with V-shaped notch and a share of a tough constituent in fracture of specimens of DWTT type, the mentioned pipes were completely removed from the manufacture.

The methodological approaches to the determination of condition of material of operating main gas pipelines are given in [1].

Material of pipes after the long-term service and pipes of emergency stock was investigated according to the requirements of technical specifications by which they were manufactured, and also to the present requirements (SNiP 2.05.06–85) taking into account the criteria of evaluation of resistance to initiation and propagation of tough and brittle fractures.

The standard main strength and ductile properties, characteristics of toughness, cold resistance, resistance to avalanche (on full-thickness specimens of DWTT type), and also structural peculiarities of metal condition have been defined.

Resistance to initiation and stable propagation of a tough crack was determined using the deformation

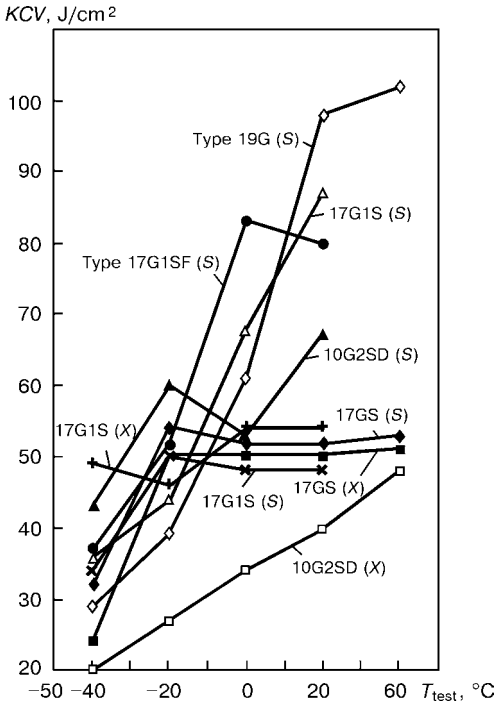

Figure 2. Impact strength of parent metal of pipes investigated

criteria: opening of defect tip at the moment of initiating a tough crack δ_i and angle of tough crack opening tg α at its stable propagation [4].

The possible change in different characteristics of pipe metal as regards to its initial condition was evaluated. The properties of pipe metal in this condition were determined on the basis of analysis of requirements of standardized documentation, processing of data of certificates. The test results of emergency stock pipes were also taken into account in determination of effect of service loads.

Chemical composition of metal of pipes made from all the steels investigated corresponded to rated requirements from the results of control analysis, while the structural parameters of parent metal and weld metals were mainly typical of used grades of steels and types of welded joints.

Results of mechanical tests of parent metal specimens are given in Figures 1–3.

Experiments showed that all the service characteristics of the parent metal of pipes (except seamless) satisfied, after a long-term service, the requirements of the standardized documentation in accordance with which they were manufactured, and located in the field of scattering or at the level of similar characteristics of metal of as-initial pipes. This also refers to the emergency stock pipes.

Metal of seamless 508 mm diameter pipe of Czechoslovakian manufacture has decreased values of yield and ultimate strength. The mentioned deviations are specified by insufficient alloying of steel of the seamless pipe, the standardized requirements to which were limited only in the upper values (C ≤ 0.18 %, Mn ≤ 1.5 %). The decreased initial strength was also promoted by a coarse-grained structure of metal of the given pipe. It should be noted that the strength

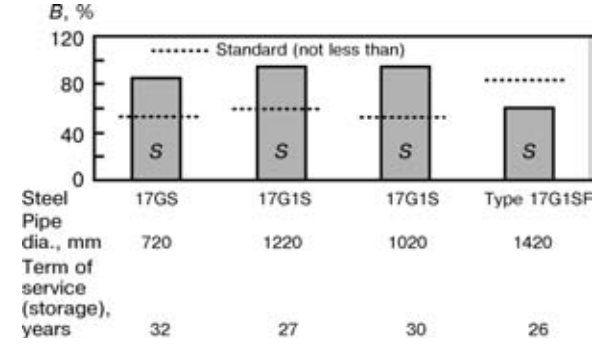

Figure 3. Share of a tough constituent B in fracture of specimens DWTT at test temperature 0 °C

characteristics of metal of separate welded pipes, in particular σ_y of metal of 1020 mm diameter pipe made from steel 17G1S and σ_t of metal of 720 mm diameter pipe made from steel 17GS, are located at the lower boundary level of corresponding requirements (see Figure 1) that proves in general the insufficient guarantees of strength of metal of pipes of a corresponding period of their manufacture.

Metal of specimens with a sharp notch within the +60 – –40 °C temperature range possesses a sufficient impact strength up to temperature –20 °C for all the pipes examined, except the emergence stock pipe made from steel 10G2SD (see Figure 2). The value of impact strength in metal of the above-mentioned pipe corresponds to the lower level required by the present standards. Temperature of transition to the brittle state of metal of the as-examined pipes was 0 °C and lower, except the seamless pipe with 20 °C temperature of transition to the brittle state of metal.

As a whole, the impact strength of metal of pipes after the long-term service and pipes of the emergency stock is little differed from its certificate values for the corresponding materials.

It should be noted that the properties of metal of pipes which were under the service do not differ significantly from those of metal of emergency stock pipes (after a long-time storage).

Resistance to avalanche fracture, evaluated by the share of a tough constituent in the fracture of DWTT specimens, corresponds to rates of SNiP 2.05.06–85 not in all as-examined pipes (Figure 3). In particular, the decreased fracture resistance at temperature 0 °C was revealed in metal of 1420 mm diameter pipe of German manufacture.

Table 1. Characteristics of metal of pipes investigated

Steel grade	*Condition of pipe metal*	ε_t, %	σ_y/σ_t	δ_i, *mm*	n	$tg\,\alpha$
17GS	*S*	18.0	0.68	0.10	0.15	0.15
	X	16.0	0.71	0.08	0.13	0.12
10G2SD	*S*	19.8	0.72	0.09	0.17	0.15
	X	19.3	0.64	0.07	0.16	0.17
Type 19G	*S*	18.8	0.58	0.17	0.15	0.19
Type 17G1SF	*X*	11.6	0.70	0.10	0.10	0.11
17G1S (∅ 1020 mm)	*S*	14.0	0.67	0.08	0.12	0.12
17G1S (∅ 1220 mm)	*X*	18.8	0.74	0.13	0.15	0.14

Characteristics of resistance to tough fractures of metal of pipes are given in Table 1. It is evident that the deformation characteristics of metal crack resistance of pipes investigated δ_i is located within the ranges typical of the low-alloy steels [5]. Somewhat decreased values of the mentioned characteristics are revealed in metal of pipes of German manufacture.

Fracture modulus or critical angle of opening of the tough crack lips tg α corresponds also to the ranges typical of investigated types of steel.

Consequently, a noticeable deterioration of crack resistance of metal of pipes after the long-term service was not observed. Comparatively low values σ_y/σ_t and corresponding increased characteristics of a deformational strengthening n, and also the values of a uniform critical deformation prove the feasibility of providing a sufficient deformability of metal in the conditions of pipes loading.

Metal of welded joints of all the pipes investigated (except one) satisfies with a sufficient reserve the established requirements to strength and toughness properties (Table 2, Figure 4). Low strength of welded joint, fractured in parent metal, of 1020 mm diameter pipe made from steel 17G1S (NPP manufacture) was caused by a decreased level of strength properties of the parent metal.

Thus, the results of carried out investigations confirm the feasibility of preserving service properties of metal of pipelines under the conditions of long-time force loading (during the scheduled and even extrascheduled terms of service).

At the long-term service the performance of the gas pipelines will be defined not only by a general deterioration of properties of pipe material due to ageing, but mostly by other factors promoting a local damage of the material.

As has been already mentioned, the pipes were manufactured earlier without taking into account the present requirements. Nevertheless, hot-rolled and normalized pipe steels of the first generations, whose specimens were investigated in work [2] and in the present work, correspond in most cases to the conditions of service of gas pipelines in the regions with moderate climate (including Ukraine). From the point of view of assurance of service properties of metal the most danger can be caused by 1420 mm diameter gas pipelines, constructed using pipes made from normalized steels. Really, as it follows from the given data, the metal of these pipes (German manufacture) is not quite reliable as to the resistance to avalanche fracture.

Revealing and removal of defects, reducing the strength of pipelines, acquire a special importance for pipes of former manufacture with insufficient technological guarantees of required quality. Defects in the zones of cold deforming can be of a great hazard because the resistance to fracture of pipe metal is deteriorated noticeably in this case.

When discussing results of investigations carried out it is rational, in our opinion, to dwell on some problems of a general nature, which refer, first of all, to the methodology of determination of material condition of the operating main pipelines. Different evaluations of phenomena of metal ageing of pipelines prove, first of all, the complexity of this problem and great difficulties in prediction of consequences of the long-term service. This confirms the opinion, expressed in [1], about the expediency in differential approach to the evaluation of current condition of metal of operating pipelines depending on definite service conditions, external actions, initial characteristics of the material and others.

In most investigations a negligible influence of service conditions on standard mechanical properties of pipe metal is noted. This almost levels the value of metal ageing factor in calculations of strength of main pipelines using traditionally accepted approaches. This evaluation is acceptable only for the material without defects, capable to plastic (tough) fracture at preset temperature-force loads.

As to the old pipelines, moreover, with decreased values of characteristics of resistance to metal fracture, then this approach to the evaluation of strength is insufficient. Using real residual properties of metal of pipes, it is necessary to perform the calculated evaluation of strength of the pipeline with such defects of metal, whose parameters are considered acceptable according to the existing standardized documentation.

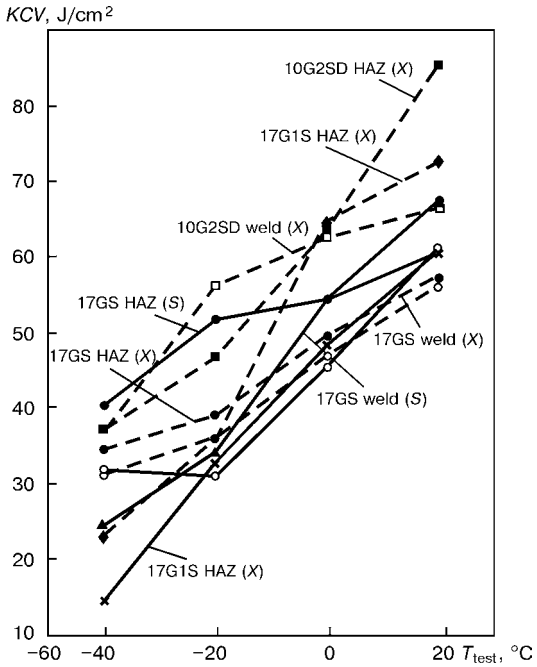

Figure 4. Impact strength of metal of longitudinal welded joints of pipes investigated

Solution of this and other similar problems requires an integrated standardized and technological support, including procedures of calculated evaluation of strength, determination of parameters of defectness and properties of the material, rules of examination, restoration of damaged areas and others.

If to consider the effect of time factor, then almost in all cases there are no specimens-witnesses, on the basis of which it would be possible to make the more

Table 2. Mechanical properties of metal of longitudinal welded joints of pipes investigated

Steel grade	*Pipe condition*	σ_t, *MPa*	KCU^{-40}, *J/cm²*	
			Weld metal	*HAZ metal*
17GS	*S*	551.0–551.6 / 551.3	60.7–67.7 / 65.3	60.8–68.5 / 63.2
	X	551.3–559.5 / 555.3	50.8–64.8 / 58.0	69.1–76.7 / 71.2
	C	511.0–617.4 / 571.9	Not determined	
10G2SD	*X*	524.3–524.4 / 524.4	76.6–97.6 / 87.1	60.8–68.5 / 63.2
	C	555.0–570.0 / 563.0	41.0–136.5* / 75.0	Not determined
Type 17G1SF	*S*	595.9–606.1 / 601.0	47.1–53.0** / 54.3	43.5–62.5** / 53.5
	C	650.0–694.0 / 688.0	42.0–57.0** / 53.0	Not determined
17G1S (∅ 1020 mm)	*X*	498.0–499.0 / 499.0	71.6–73.3 / 72.3	61.6–72.3 / 67.0
17G1S (∅ 1220 mm)	*S*	533.0–533.0 / 533.0	25.5–38.0 / 31.7	63.0–65.6 / 64.3
	C	558.2–583.0 / 568.4	Not determined	

*At temperature −20 °C.
**At temperature −55 °C.

valid evaluation of changes in parameters of the material condition. It is also evident, that there is no information about the initial characteristics of the material which are determined by the new test methods. It should be noted that the non-correct evaluation of the level of initial properties can lead to the erroneous conclusions concerning the consequences of ageing processes.

As was outlined in [1], some specifics of pipe metal cannot be ignored, for example, rather large scattering of initial values of mechanical properties or change in quality characteristics in different periods of time that is connected with a large scale of production of pipe steel and pipes, especially in the past years, and also with upgrading of the production technologies.

Thus, the evaluation of a current condition of metal from the point of view of its suitability to service at preset conditions should be made taking into account the level of quality of pipes of the previous production.

A particular interest is shown to the study of metal condition of separate regions of pipelines, on which the conditions are occurred due to unscheduled situations and special circumstances, promoting the metal damage caused by hydrogenation, cold plastic deformation, polyfrequency loading, different chemical-mechanical actions.

The variety of possible phenomena requires conductance of the more comprehensive investigations to reveal the specific features which accompany different processes of ageing. Complex of these investigations comes out beyond the scope of control and test procedure in manufacture of pipe products.

Classification of conditions of the material can be of significant help in the solution of these problems, for example on the basis of the approach given in [1]. In our opinion, it is rational to develop further the scale of limiting parameters characterizing the serviceable, partially serviceable and pre-emergency condition of the material for typical groups of pipe steels.

CONCLUSIONS

1. The investigations carried out on specimens of parent metal and welded joints cut from «old» main gas pipelines, laid at the territory of Ukraine, confirmed after up to 35 years service the feasibility of preserving acceptable service properties of pipe metal in scheduled and even extrscheduled terms of service. Thus, to ensure the long-time service reliability of «old» gas pipelines it is very important to reveal and remove the hazardous defects in metal of pipes and welded joints.

2. Due to imperfection of complex of initial technical requirements to pipes, the evaluation of condition of operating gas pipelines (or regions of gas pipelines), in construction of which in the 1950–1970s the pipes were used with an insufficient technological guarantees of quality, deserves a special attention. Identification of laid pipes, evaluation of the level of technical characteristics and stability of quality of used materials has a great importance in diagnostic examination and rehabilitation of these gas pipeline.

1. Paton, B.E., Semyonov, S.E., Rybakov, A.A. et al. (2000) Ageing and procedure of evaluation of the state of metal of the main pipelines in service. *The Paton Welding J.*, **7**, 2–10.
2. Semyonov, S.E., Rybakov, A.A., Kirian, V.I. et al. (2001) Experimental evaluation of the state of metal of long-serviced welded oil pipelines. *Ibid.*, **5**, 17–21.
3. Lejkin, I.M., Litvinenko, D.A., Rudchenko, A.V. (1972) *Production and properties of low-alloy steels*. Moscow: Metallurgiya.
4. Girenko, V.S., Semyonov, S.E., Goncharenko, L.V. (2001) Strain ageing of pipe steels. *Tekhn. Diagnostika i Nerazr. Kontrol*, **3**, 32-35.
5. Paton, B.E., Trufyakov, V.I., Kirian, V.I. (1982) Requirements to viscosity of steel for main gas pipelines in use of avalanche fracture arresters in them. *Avtomatich. Svarka*, **12**, 5–7.

SPECIAL FEATURES OF CAPILLARY WAVES IN THE VAPOUR-GAS CHANNEL IN ELECTRON BEAM WELDING OF THICK METAL

V.M. NESTERENKOV
E.O. Paton Electric Welding Institute, NASU, Kyiv, Ukraine

Features of natural oscillations of liquid metal on the vapour-gas channel walls have been studied. It is shown that in welding with a uniformly-moving electron beam capillary waves form on the melt surface under the impact of reaction force of recoil pressure, arising as a result of electron beam interaction with the channel front wall. These capillary forces have a discrete spectrum of natural frequencies, the density of which increases with the penetration depth. A variance relation has been derived for the capillary waves on the inner surface of a cylindrical channel. Such low-frequency oscillations of the melt may result in instability of the welding process.

Key words: *electron beam welding, vapour-gas channel, capillary waves, hydrodynamic stability, laminar flow, spectrum of natural oscillations, variance relation, damping coefficient*

As indicated by numerous experimental data [1], hydrodynamic stability of molten metal in the vapour-gas channel is important for normal running of the welding process and producing sound welds. Contrarily, oscillations of the surface of the melt, arising against the background of total motion of liquid metal in the weld pool, may lead to inhomogeneity of welded joints, and formation of various defects of the type of root defects, false channel, or blowholes. The role of such oscillations of melt surface in weld formation increases with the increase of the thickness of metals being welded above 80 mm [2]. As in EBW of metals of average or even small thickness difficulties are also encountered in producing sound joints [3], this paper provides analysis of the features of natural oscillations of liquid metal on the walls of the vapour-gas channel and singles out those of them, which determine the parameters of the technology of EBW of thick metals and alloys.

In view of the fact that various turbulences, arising in the melt flowing along the walls of vapour-gas channel, impair its hydrodynamic stability (and, as a result, the quality of the welded joint as a whole), in order to provide the maximum stability of the welding process it is necessary for the melt motion inside the channel to be laminar. It is known from practice, that the diameter of the vapour-gas channel d, as a rule, is much smaller than its depth H ($d << H$). Therefore, the known from hydrodynamics analogy of liquid flowing around a simple or elliptical long cylinder can be used to analyze the melt motion in the channel [4]. The greater the channel depth, the more valid will such a description be, particularly, at complete penetration. In this case, in view of the smallness of the coefficient of kinematic viscosity of molten metal at high temperatures ($\nu \approx 10^{-3}$–10^{-2} cm^2/s), the motion of liquid metal along the surface of vapour-gas channel may be regarded as dissipation-free, considering the viscosity to be different from zero only in the layer adjacent to the solid wall of the channel. In this case, the melt motion along the walls of the vapour-gas channel may be regarded as a potential one, i.e. a flow described by one function — potential of velocities Φ_0, related in each point of the melt to the components of the velocity vector $\mathbf{v}_i$ by the following relationship [5]:

$$\mathbf{v}_i = \partial\Phi_0 / dx_i, \qquad (1)$$

where x_i are the space coordinates (i = 1, 2, 3).

Thus, the melt velocity is determined as a gradient of function Φ_0. From the condition of continuity of incompressible liquid it follows that the potential of velocities Φ_0 should satisfy Laplace equation in the entire melt volume

$$\Delta\Phi_0 = 0, \qquad (2)$$

where Δ is the Laplace operator.

In terms of interaction of the electron beam with the walls of the vapour-gas channel, the disturbances arising on the channel wall (particularly on the front wall) are important. A number of publications [6, 7] deal with waves on the edge of a continuous cylinder of liquid metal, but the issue of capillary waves on the internal surface of the vapour-gas channel remained untreated. Analysis of the influence of such waves on the channel stability and weld formation in EBW is of great practical interest.

Considering the melt to be an incompressible liquid and neglecting the kinetic energy ($v^2/2$) as the term of the second order of smallness, let us write according to [5] the equation for a disturbed increment of velocity potential Φ in the vapour-gas channel:

$$p = -\rho g z - \rho \frac{\partial\Phi}{\partial t}, \qquad (3)$$

where p is the melt pressure in the channel near its surface at depth z; ρ is the density of the molten

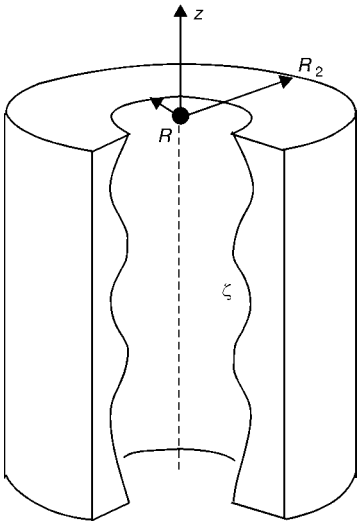

Figure 1. Capillary waves on the melt surface ξ inside the vapour-gas channel in the form of a hollow cylinder of radii R and R_2

metal; g is the gravity acceleration; Φ is the difference between the disturbed and undisturbed velocity potentials; z is the coordinate in the vertical direction, counted from the channel upper edge.

Pressure p in the melt near the gas–liquid interphase is defined as the difference between the pressure on the melt surface inside the vapour-gas channel p_c and Laplace pressure

$$p = p_c - \frac{\sigma}{R}, \qquad (4)$$

where σ is the surface tension coefficient of liquid metal; R is the inner radius of vapour-gas channel; $p_c = p_c(r, t)$ is the pressure in the channel (in the general case the function of coordinates and time). In turn, pressure on the melt surface inside the channel p_c consists of the pressure of gas and vapours of metal in the channel p_v and recoil pressure p_r, resulting from metal evaporation from the melt surface under the impact of the electron beam.

At static limit formula (3) turns into the known condition of equilibrium for the vertical vapour-gas channel [8]

$$p_c = \frac{\sigma}{R} - \rho g z. \qquad (5)$$

As small disturbances ζ formed on the free surface of the melt inside the channel, are directed along a normal to the surface proper, in the case of a vertical vapour-gas channel, they do not affect the gravity component of equation (3). Deducing from (3) a similar equation for a disturbed potential and neglecting the terms of the second order of smallness, for a disturbed increment of velocity potential Φ at $r = R$, we have the following equation:

$$\frac{\partial \Phi}{\partial t} + \frac{\sigma}{\rho}\left(\frac{1}{R_s} + \frac{1}{R}\right) + \frac{\Delta p_c}{\rho} = 0, \qquad (6)$$

where Δp_c is the difference between the disturbed and undisturbed pressure on the melt surface in the channel; R_s and R is the radius of curvature of the disturbed and undisturbed surface of the melt, respectively.

After differentiating equation (6) with respect to time, we come to the next equation for Φ on the melt surface inside the channel:

$$\left\{\frac{\partial^2 \Phi}{\partial t^2} + \frac{\sigma}{\rho}\frac{\partial}{\partial t}\left(\frac{1}{R_s}\right) + \frac{\partial}{\partial t}\left(\frac{\Delta p_c}{\rho}\right)\right\}_{r = R} = 0. \qquad (7)$$

In welding with a uniformly moving electron beam pressure p_c, applied to the walls of vapour-gas channel, changes only slightly in a quasi-stationary welding process. Therefore, in the first approximation the last term in equation (7) may be neglected. Then, solution of this equation is reduced to a problem of the natural oscillations of the melt in the vapour-gas channel. For this purpose, it is necessary to determine curvature radius R_s of the melt inner surface, which is not greatly different from a cylindrical surface in the first approximation. In this case, the shape of liquid metal on the channel walls may be presented as a hollow cylinder with the inner and outer radii R and R_2, respectively (Figure 1). Disturbance of the melt surface inside the channel ζ will change along the channel depth along axis z, which may result in capillary waves propagating over the channel surface. R_s may be determined by minimizing the area of inner surface of a cylinder. Surface area S, described by function $r = r(\varphi, z)$, in the cylindrical coordinates may be represented in the following form [9]:

$$S = \int_0^{2\pi} \int_0^{H} \sqrt{1 + \left(\frac{1}{r}\frac{\partial r}{\partial \varphi}\right)^2 + \left(\frac{\partial r}{\partial z}\right)^2}\, r d\varphi dz, \qquad (8)$$

where φ is the horizontal angle.

Cylindrical surface is assigned by equation $r = R = \text{const}$, and a surface close to it, slightly different from a cylindrical one, is described by equation $r = R - \zeta$ with a small ζ. Substituting this value in formula (8), we will approximately have

$$S = \int_0^{2\pi H} \int_0^{} \left\{(R - \zeta) + \frac{1}{2(R - \zeta)}\left(\frac{\partial \zeta}{\partial \varphi}\right)^2 + \frac{(R - \zeta)}{2}\left(\frac{\partial \zeta}{\partial z}\right)^2\right\} d\varphi dz. \qquad (9)$$

Solving the problem of S minimization by variation of functional [5] with an accuracy to the terms of the first order of smallness by ζ, we obtain

$$\frac{1}{R_s} = -\frac{1}{R}\left(1 + \frac{\zeta}{R} + \frac{1}{R}\frac{\partial^2 \zeta}{\partial^2 \varphi} + R\frac{\partial^2 \zeta}{\partial^2 z}\right). \qquad (10)$$

Substituting formula (10) into equation (7), after time differentiation we get

$$\frac{\partial^2 \Phi}{\partial t^2} = \frac{\sigma}{\rho R}\frac{\partial}{\partial t}\left(1 + \frac{\zeta}{R} + \frac{1}{R}\frac{\partial^2 \zeta}{\partial^2 \varphi} + R\frac{\partial^2 \zeta}{\partial^2 z}\right). \qquad (11)$$

Using a kinematic boundary condition on the inner surface of a cylinder

$$v_r = \frac{\partial \Phi}{\partial r}\Big|_{r=R} = -\frac{\partial \zeta}{\partial t}, \quad (12)$$

we obtain the following condition for velocity potential Φ at $r = R$:

$$\frac{\partial^2 \Phi}{\partial t^2} = -\frac{\sigma}{\rho R^2}\frac{\partial}{\partial r}\left(\Phi + \frac{\partial^2 \Phi}{\partial^2 \varphi} + R^2 \frac{\partial^2 \Phi}{\partial^2 z}\right)_{r=R}. \quad (13)$$

A complex solution of equation (13) in the form of a standing wave

$$\Phi = \exp(-i\omega t) f(r, \varphi, z), \quad (14)$$

where ω is the frequency of natural oscillations; t is the time; function $f(r, \varphi, z)$, expressed in cylindrical coordinates, satisfies Laplace equation (2) in the entire volume of a liquid cylinder.

As is known [9], solution of Laplace equation for a cylinder can be represented in the following form:

$$f = \exp[\pm i(kz + m\varphi)] M_m(kr), \quad (15)$$

where k is the wave vector; m is the integer number; M_m is the linear combination of modified Bessel functions of the first and second kind $I_m(kr)$ and $K_m(kr)$:

$$M_m(kr) = [A_m I_m(kr) + B_m K_m(kr)]; \quad (16)$$

A_m, B_m are the coefficients, determined from boundary conditions.

Solution of kind (15) admits propagation of sinusoidal waves along the inner surface of a hollow cylinder. Using an additional kinematic boundary condition for velocity potential Φ on the outer surface of a cylinder ($r = R_2$)

$$v_r = \frac{\partial \Phi}{\partial r}\Big|_{r=R_2} = 0, \quad (17)$$

coefficient B_m may be eliminated from formula (16). This boundary condition means that the radial component of melt velocity turns to zero on the solid wall of vapour-gas channel. Then formula (16) becomes

$$M_m(kr) = A_m\left[I_m(kr) - K_m(kr)\frac{I'_m(kR_2)}{K'_m(kR_2)}\right], \quad (18)$$

where $I'_m(KR_2)$ and $K'_m(kR_2)$ are the derivatives of modified Bessel functions of the first and second kind, respectively.

Substituting Φ in the form of (14) into equation (13), we obtain the following boundary condition at $r = R$:

$$\frac{\partial^2 \Phi}{\partial t^2} = \frac{\sigma}{\rho R^2}[(m^2 + k^2R^2) - 1]\left(\frac{\partial \Phi}{\partial r}\right)_{r=R}. \quad (19)$$

Some simplification in equation (19), using formulas (14) and (15) yields a variance relation for a hollow cylinder:

$$\omega_m^2 = \frac{\sigma}{\rho}\frac{k}{R^2}[1 - (k^2R^2 + m^2)]\frac{\partial M_m(kr)}{\partial(kr)}\Big|_{r=R}\frac{1}{M_m(kR)}, \quad (20)$$

where ω_m is the frequency of m^{th} mode of natural oscillations.

Having differentiated multiplier $M_m(kr)$ with respect to radius r and substituted the derived expression into equation (20), we obtain the following variance relation:

$$\omega_m^2 = \frac{\sigma}{\rho}\frac{k}{R^2}[(k^2R^2 + m^2) - 1]\, C_m, \quad (21)$$

where $C_m = C_m(k, R, R_2)$ is the multiplier, dependent on wave vector k and parameters of vapour-gas channel R and R_2, which has the following form:

$$C_m(k, R, R_2) = \frac{[K'_m(kR)I'_m(kR_2) - I'_m(kR)K'_m(kR_2)]}{[I_m(kR)K'_m(kR_2) - K_m(kR)I'_m(kR_2)]}. \quad (22)$$

It should noted that relation (21) is fundamentally different from a similar one for waves of a flat surface of a cylinder, first of all, by the presence of multiplier C_m and, secondly, by the presence of an instability zone for zero ($m = 0$) natural oscillations, as at $kR < 1$ value ω_0 becomes purely imaginary ($\omega_0^2 < 0$).

Taking into account the variance relation (21), boundary condition (19) can be written in the following form:

$$\left\{\frac{\partial^2 \Phi}{\partial t^2} + \omega_m^2 \Phi\right\}_{r=R} = 0. \quad (23)$$

Relationship (23) is an equation of natural oscillations of melt surface in the vapour-gas channel. The situation, when melt oscillations are defined by equation (23) is in place, for instance, in welding with a uniformly moving electron beam. Without electron beam scanning the pressure, applied to the channel front wall, changes only slightly during the quasistationary welding process, and melt oscillations proceed at natural frequencies.

As in the actual welding process the electron beam (or workpiece) are moving in a certain direction, in welding with a uniformly moving beam first of all the first mode of melt oscillations is excited in the vapour-gas channel ($m = 1$), which corresponds to longitudinal oscillations of the melt of the type of displacements in the welding direction. For the first oscillation mode variance relation (21) becomes

$$\omega_1^2 = C_1\frac{\sigma k^3}{\rho}, \quad (24)$$

where $C_1 = C_1(k, R, R_2)$ is the coefficient, found from formula (22) at $m = 1$. This means that at high values of k the spectrum of melt oscillations in the vapour-gas channel is described by the exponential law: $\omega \sim k^{3/2}$. Coefficient of surface tension σ and melt density ρ, incorporated into formulas (24) and (21), are temperature functions. These values decrease with temperature increase, so that the frequency of natural oscillations ω, proportional to just their relationship ($\omega \sim \sqrt{\sigma/\rho}$), changes only slightly in the temperature interval of $T_m < T < T_b$, where T_m and

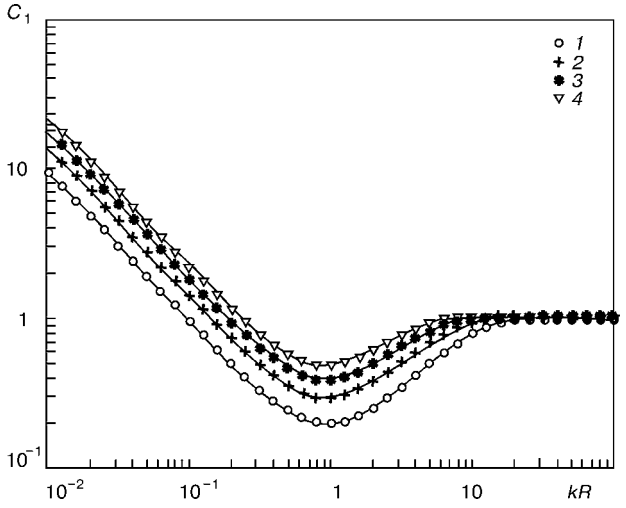

Figure 2. Dependence of coefficient $C_1 = f(kR)$ for the first mode of natural oscillations of the melt ($m = 1$) in a cylindrical vapour-gas channel at different parameters of the channel: $R_2/R = 1.10$ (*1*), 1.15 (*2*), 1.20 (*3*) and 1.25 (*4*)

T_b are the temperatures of metal melting and boiling, respectively. Therefore, in ω_1 determination the temperature dependencies of these values can be ignored in the first approximation. Let us analyze multiplier C_1 in formula (24). Figure 2 gives dependencies $C_1 = f(kR)$ for $m = 1$ in the vapour-gas channel with outer radius $R_2 = 2.75$ mm at different values of parameter $R_2/R = 1.10, 1.15, 1.20, 1.25$. It is seen from the Figure that, first, with increase of wave vector k value C_1 first drops quickly, reaching a minimum at $kR \approx 1$, and then grows, tending to zero ($C_1 \to 1$) at $k \to \infty$. Secondly, with decrease of channel inner radius R (and, hence, increase of the thickness of the melt layer on the walls of vapour-gas channel $d = R_2 - R$) value C_1 in the long-wave part of the spectrum also rises.

Each mode of melt oscillations in the vapour-gas channel of a finite depth corresponds to a whole set of natural oscillation frequencies. Such a discreteness of the spectrum of natural oscillations of the melt follows from the fact that the potential of velocities Φ, in addition to Laplace equations, should also satisfy the boundary conditions at the bottom and on top of vapour-gas channel

$$\frac{\partial \Phi}{\partial z}\Big|_{z=-H} = 0, \quad \frac{\partial \Phi}{\partial z}\Big|_{z=0} = v_z, \tag{25}$$

where v_z is the melt velocity on a free horizontal surface of the melt.

Values of wave vectors and natural frequencies for the first mode ($m = 1$) of oscillation of the melt surface in the vapour-gas channel at different penetration depths

H, mm	k_1, cm^{-1}	Δk, cm^{-1}	ω_1, rad/s	f_1, Hz
50	0.314	0.628	3.38	0.54
75	0.209	0.419	2.25	0.36
100	0.157	0.314	1.69	0.27
125	0.126	0.251	1.35	0.21
150	0.105	0.209	1.12	0.18

These boundary conditions are similar to the known conditions for vibration of a string or membrane with one end fixed and one free, and mean that a certain number of oscillations should fit along the entire length of channel H. Therefore, for a wave vector k of the n^{th} harmonic the following relation should hold:

$$k_n H = \left(n - \frac{1}{2}\right)\pi, \tag{26}$$

where n is the number of oscillation harmonics, $n = 1, 2, 3, \ldots$. For instance, for $n = 1$ we obtain a value of wave vector $k_1 = \pi/2H$, which corresponds to oscillation quarter-wave.

From formulas (24) and (26) it follows, in particular, that with increase of penetration depth H the values of wave vectors k_n for all the melt oscillation harmonics shift towards smaller values (which corresponds to shifting of the entire oscillations spectrum to the low-frequency range), and the interval between the adjacent values of natural frequencies ($\Delta\omega_n = \omega_{n+1} - \omega_n$) becomes smaller. The Table gives the values of wave vectors and corresponding values of the smallest natural frequency for the first oscillation mode ($m = 1$) of the iron melt ($\sigma = 1.5$ N/m and $\rho = 7.86$ g/cm^2), calculated by formula (24) at different penetration depths. It is seen from the Table that with H increase the values of natural freqencies decrease and reach a sub-Hertzian range ($f_1 \approx 0.1$ Hz). In addition, the interval between the allowed wave vectors of melt oscillations in the channel $\Delta k = k_2 - k_1$ is also reduced with increase of H, which corresponds to transition of the discrete spectrum of oscillations to a continuous one at $H \to \infty$.

Melt oscillations in the vapour-gas channel may differ not only in frequency, but also in shape. Therefore, the oscillation spectrum will consist of a whole set of natural frequencies ω_{mn}, where $m = 0, 1, 2, \ldots$ is the oscillation mode. Greater values of n correspond to higher oscillation frequencies. Mode $m = 0$ corresponds to axisymmetric oscillations on the inner surface of the vapour-gas channel of the type of constriction and expansion (Figure 3, *a*), and mode $m = 1$ corresponds to oscillations of the type of displacements and bends along a certain chosen direction, for instance, direction of welding motion (Figure 3, *b*).

Thus, in welding with a uniformly moving electron beam melt oscillations in the vapour-gas channel occur mostly at natural frequencies ω_{mn}, and the entire spectrum can be excited. On the other hand, axisymmetric oscillations ($m = 0$) lead to instability of the vapour-gas channel, starting with penetration depths H just several times greater than the channel inner radius $R/H \geq \pi nR$ [7]. This estimate does not take into account the presence of a free surface on top of the vapour-gas channel, therefore, more correct is the condition of channel instability, which follows from (26):

$$H \geq \left(n - \frac{1}{2}\pi R\right) (n = 1, 2, 3, \ldots). \qquad (27)$$

It follows from the above-said that in development of EBW technology it is necessary to take into account the limit of the lowest welding speed, lowering of which will lead to excitation of an axisymmetric mode ($m = 0$) of melt oscillations, and, as a result of it, to instability of the vapour-gas channel as a whole. Channel stability can be increased by exciting other oscillatory modes, in particular $m = 1$. This is achieved by increasing the welding speed, and, consequently, by suppression of axisymmetric oscillations of the melt. In this case the harmonics of the oscillation mode $m = 1$ are the first to become excited, corresponding to swinging of liquid metal along the direction of welding x. Such oscillations, unlike the zero mode oscillations, are stable and can occur in a wide frequency range.

Let us conduct numerical estimates of frequency ω_{11} and corresponding attenuation factor $\gamma(\omega_{11})$ for oscillations with $m = 1$ and $n = 1$. We will use for this purpose the expression for the coefficient of capillary wave attenuation [5], which in view of (24) becomes

$$\gamma = 2\nu k^2 = 2\nu \left(\frac{\rho}{\sigma}\right)^{2/3} \frac{\omega_1^{4/3}}{C_1^{2/3}}. \qquad (28)$$

Considering, that increase of penetration depth results in a shift of the spectrum of melt oscillations towards the low-frequency oscillations, the attenuation coefficient $\gamma(\omega_{1n})$ of each of the harmonics taken separately also decreases. Thus, at penetration depth $H = 50$ mm the wave vector of the first harmonics is equal to $k_1 = 0.314$ cm^{-1}. Therefore, if we take the dynamic viscosity of the iron melt of the order of $\nu_{Fe} \approx 10^{-2}$ cm^2/s, then the attenuation factor will be equal to $\gamma(\omega_{11}) = 2 \cdot 10^{-2}(0.314)^2 \approx 2 \cdot 10^{-3}$ s^{-1}, which corresponds to an extremely small weakening of the first harmonics of melt oscillations. With such an attenuation decrease of oscillation amplitude by e times proceeds over a sufficiently long time $t \approx 5 \cdot 10^{-2}$ s. Due to variation of attenuation coefficient $\gamma = \gamma(\omega)$, the high-frequency harmonics ($n >> 1$) damp out faster than the low-frequency ones. Eventually, at melt oscillations at natural frequencies the lowest harmonics ($n = 1$) will predominate, which has the maximum amplitude, for which the attenuation coefficient γ has a minimum value. Such low-frequency oscillations are always manifested as removal of molten metal from the vapour-gas channel to the weld pool surface in EBW of thick metal.

Figure 4 gives the photograph of low-frequency disturbances in the form of large rolls of metal on the surface of a weld on aluminium alloy 2024, arising in welding in the downhand position with a uniformly moving electron beam. Penetration depth at welding speed $v_w = 4$ mm/s was equal to $H = 120$ mm. The photo clearly demonstrates the periodical nature of liquid metal removal from the vapour-gas channel

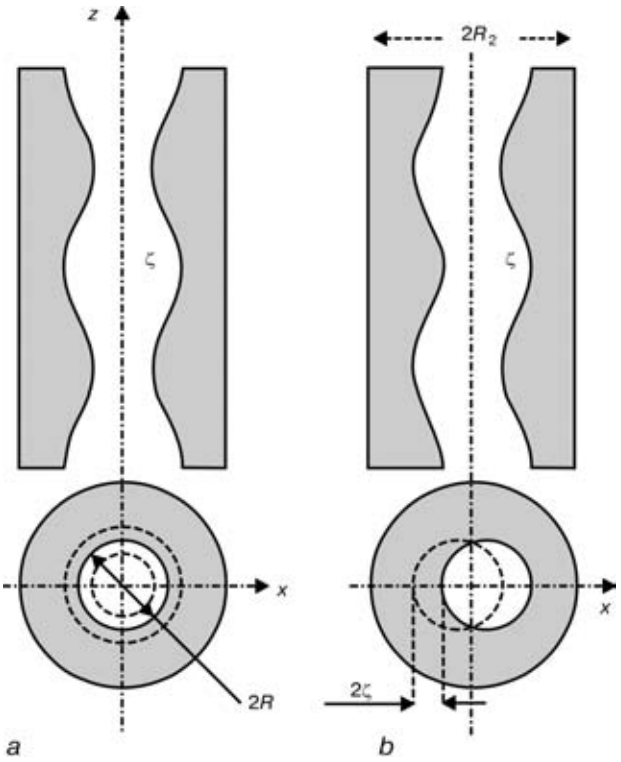

Figure 3. Modes of natural oscillations of the melt inner surface ξ in the vapour-gas channel: a — axisymmetricl constrictions ($m = 0$); b — transverse displacements ($m = 1$)

during the welding process. Let us evaluate the frequency of low-frequency oscillations shown in Figure 4, a. Using the scale of the Figure and value of welding speed (4 mm/s), we will find that the average frequency of oscillations, having the highest amplitude, $f \approx 0.33$ Hz. Let us compare the obtained value with the theoretical one, for which purpose we will substitute the known values of penetration depth of the sample ($H = 120$ mm), density ($\rho = 2.5$ g/cm^3) and surface tension coefficient ($\sigma = 0.9$ N/m) for liquid aluminium into formulas (24) and (26). In order to calculate coefficient C_1 incorporated into (24), it is necessary to know the dimensions of the vapour-gas channel R and R_2. Value of the radius of the channel outer wall R_2 can be determined rather

Figure 4. Disturbances (*top view*), arising on the surface of a weld on aluminium alloy in EBW in the downhand position at the speed of 4 mm/s: a — by static electron beam; b — with electron beam scaning ($f_1 = 180$ Hz)

accurately by the macrosection of the welded sample (for a weld shown in Figure 4, R_2 = 2.75 mm). In connection with the fact that direct measurement of inner radius of the channel is difficult to perform in practice, value R will be used as a variable parameter in calculations. The best agreement between the theoretical and experimental values of f is achieved at mean radius of melt surface inside the channel, equal to R = 2.35 mm. In this case the average thickness of melt layer on the channel walls is $d = R_2 - R \approx$ $\approx$ 0.4 mm. Substituting all the obtained values ($k_1 = \pi/2H \approx 0.131$ cm^{-1}, R = 2.35 and R_2 = 2.75 mm) into formula (22) at m = 1, we have C_1 = 5.0737. Therefore, for the lowest frequency of melt oscillations f_1 from formula (24) we obtain

$$f_1 = \frac{1}{2\pi}\sqrt{C_1 \frac{\sigma}{\rho}\left(\frac{\pi}{2H}\right)^3} \approx 0.325 \text{ (Hz)}. \qquad (29)$$

Theoretical ($f_1 \approx 0.325$ Hz) and experimental ($f_1 \approx$ $\approx$ 0.33 Hz) values for the lowest frequency of melt oscillations in the weld pool at vapour-gas channel internal radius R = 2.35 mm practically coincide, which is indicative of a good agreement of theory with experiment.

Figure 4, *b* shows the appearance of the weld, made with the same parameters as the weld in Figure 4, *a*, but using longitudinal oscillations of the beam at 180 Hz frequency. As is seen from the Figure, no periodical coarse metal rolls are observed in this case on the weld surface, which are indicative of an oscillatory nature of melt motion inside the vapour-gas channel. A practically even upper bead in Figure 4, *b*, points to a laminar nature of the liquid meal flow over the channel walls, when using electron beam scanning.

Thus, application of electron beam scanning permits, on the one hand, selective excitation of certain oscillatory modes separately from other modes (thus avoiding the unstable zero oscillation mode), and on the other hand, by selecting an appropriate frequency of electron beam oscillations, it allows reducing the amplitude of natural oscillations of the melt in the vapour-gas channel. In particular, applying a longitudinal scan, allows excitation of a stable first oscillation mode (m = 1), while suppressing the unstable zero mode (m = 0). This permits improvement of the hydrodynamic stability of the vapour-gas channel, which is manifested in a more uniform weld formation.

Melt oscillations under the action of the reaction force of recoil pressure, arising in metal evaporation from the channel front wall under the impact of the electron beam, were considered in terms of the proposed model of the vapour-gas channel. It is shown that in welding with a uniformly moving electron beam disturbances (capillary waves) arise on the melt inner surface in the vapour-gas channel. These disturbances have a discrete oscillation spectrum, where the density rises with the increase of the penetration depth. Amplitude of melt oscillations in the channel depends on the frequency of natural oscillations, and reaches the maximum value at the lowest allowed frequency.

A variance relation $\omega = \omega(k)$ has been derived for capillary waves on the inner surface of the vapour-gas channel, which differs from the known relation for waves on the edge of a cylinder. It is shown that due to variance of the attenuation coefficient of the capillary waves $\gamma = f(\omega)$, the first harmonics of natural oscillations of the melt (n = 1) turns out to be the most long-lived. This harmonics has the lowest frequency and the highest amplitude, and its existence is confirmed experimentally. Such low-frequency oscillations of the melt in the vapour-gas channel may lead to instability of the welding process, which is related to the molten metal penetration directly under the electron beam, and, hence, to formation of different defects in welds.

To stabilize the melt motion in vapour-gas channels of a great depth ($\geq$ 80 mm) is recommended to apply electron beam scanning at a maximum possible frequency, the value of which is limited from above by the attenuation in the viscous layer of liquid metal, adjacent to the solid wall of the weld pool.

1. Nazarenko, O.K., Kajdalov, A.A., Kovbasenko, S.N. et al. (1987) *Electron beam welding*. Ed. by B.E. Paton. Kyiv: Naukova Dumka.
2. Paton, B.E., Leskov, G.I., Nesterenkov, V.M. (1988) Dynamic models of penetration channels in electron beam welding. *Avtomatich. Svarka*, **1**, 1–6.
3. Ryzhkov, F.N., Postnikov, V.S. (1963) Electron beam welding with longitudinal oscillations of the electron beam. *Ibid.*, **11**, 43–47.
4. Yablonsky, V.S. (1961) *Short course of technical hydromechanics*. Moscow: Fizmatgiz.
5. Landau, L.D., Lifshits, E.M. (1954) *Mechanics of continua*. Moscow: Gostekhizdat.
6. Akopyants, K.S., Nesterenkov, V.M., Nazarenko, O.K. (2002) Electron beam welding of 60 mm thick steels using longitudinal oscillations of beam. *The Paton Welding J.*, **9**, 2–4.
7. Maruo, H., Hirata, Y. (1993) Natural frequency and oscillation mode of weld pool. *Quarterly J. JWS*, **1**, 50–54.
8. Sudnik, V.A., Radai, D., Erofeev, V.A. (1997) Computer modelling of laser welding: model and verification. *Svarochn. Proizvodstvo*, **1**, 28–33.
9. Korn, G., Korn, T. (1974) *Refer. book on mathematics*. Moscow: Nauka.

TOWARDS THE PROBLEM OF FORMATION OF LONGITUDINAL CRACKS IN WELDED JOINTS OF HIGH-STRENGTH STEELS

L.M. LOBANOV, L.I. MIKHODUJ, V.D. POZNYAKOV, O.L. MIKHODUJ, V.G. VASILIEV and **P.A. STRIZHAK**
E.O. Paton Electric Welding Institute, NASU, Kyiv, Ukraine

Technological sample and procedure of investigations have been developed that makes it possible to evaluate the effect of residual stresses on resistance of welded joints with multilayer welds to the initiation of longitudinal cold cracks. The resistance to the initiation of longitudinal cold cracks in 14KhGN2MDAFB steel welded joints, made by wire Sv-10KhGN2SMFTYu in mixture of gases Ar + 20 % CO_2, was evaluated with allowance for the level of residual stresses.

Key words: *residual welding stresses, low-carbon alloy steel, structural transformations, delayed fracture, yield strength, ductility*

In domestic and foreign practice the low-carbon (≤ 0.2 % C) high-strength steels with 600–1000 MPa yield strength find the wide application in manufacture of critical welded structures. As the experience showed, their rational application can greatly improve the technical-economical characteristics of the machines, mechanisms and engineering constructions. The major problems in welding of these steels are connected with the prevention of a delayed fracture in welded joints. As is known, the structure of weld and HAZ metal, concentration of diffusive hydrogen, welding stresses in joints influence significantly this process.

As regards to low-carbon high-strength steels the domestic and foreign researches investigated comprehensively two main causes of a delayed fracture: hydrogen and structural factors. When it was possible, they also took into account the action of residual stresses. The wider study of effect of the latter on the process of initiation and propagation of cold cracks is hindered by methodological difficulties stipulated by high strength properties and values of hardness of welded joints, and also by complex structural transformations proceeding in metal of weld and HAZ during cooling. As a rule, they lead, from the one hand, to a significant increase in strength properties, and, from the other hand, to the proceeding of rather complex phase-structural transformations. All these factors can greatly influence the level of stresses in welded joints made from the alloy steels.

The capabilities of advanced methods of investigations of weldability enable us to analyze these processes to a certain extent. This refers first of all to the simulation of thermal welding cycles on samples of large enough sizes, dilatometric examinations, high-temperature tests and others. Later on these approaches can be supplemented and clarified by the analysis of residual stresses on real welded joints using the method of holographic interferometry or other methods of examinations [1, 2].

High-strength alloy steels of 12GN2MFAYu, 14KhG2SAFD, 12GN3MFAYuDR, 14KhGN2MDAFB, 12KhGN2MFBDAYu and 12KhGN2MFDRA grades with $\sigma_{0.2}$ = 630–850 MPa served as a base for these investigations (Table 1). Almost all of them were developed in the 1970–1980s in I.P. Bardin Central Research Institute of Ferrous Metals and N.P. Melnikov Central Research Institute of Designing Welded Structures [3–5]. The mentioned steels contain up to 0.17 % C, complex-alloyed with Mn, Cr, Ni, Mo and other elements (at a total content of 4–6 %). In the process of production they are subjected to heat treatment (quenching and tempering).

Table 1. Chemical composition and mechanical properties of high-strength alloy steels

Steel grade	*Elements, wt.%*										
	C	*Si*	*Mn*	*Cr*	*Ni*	*Mo*	*Cu*	*Al*	N_2	*V*	*B*
12GN2MFAYu (VS-1)	0.12	0.50	1.20	0.50	1.50	0.19	–	0.10	0.027	0.07	–
14KhG2SAFD	0.13	0.57	1.42	0.44	0.16	0.03	0.39	0.08	–	0.08	–
12GN3MFAYuDR	0.12	0.23	1.26	–	3.08	0.33	0.40	0.02	0.015	0.05	0.003
14KhGN2MDAFB	0.15	0.23	1.30	0.97	2.20	0.33	0.41	0.07	0.015	0.14	–
12KhGN2MFBDAYu	0.13	0.41	1.11	0.76	1.63	0.53	0.55	0.03	0.020	0.08	–
12KhGN2MFDRA	0.12	0.32	1.10	1.08	2.00	0.52	0.60	–	–	0.10	0.002

Table 1 (cont.)

Steel grade	P^*_{cm}	Mechanical properties			
		$\sigma_{0.2}$, MPa	T_{test}, °C	KCU, J/cm^2	KCV, J/cm^2
12GN2MFAYu (VS-1)	0.270	628	–70	46	–
14KhG2SAFD	0.340	635	–40	43	–
12GN3MFAYuDR	0.303	768	–70	–	72
14KhGN2MDAFB	0.372	752	–40	–	75
12KhGN2MFBDAYu	0.334	828	–70	47	–
12KhGN2MFDRA	0.356	849	–50	–	30

$^*P_{cm} = C + \frac{Si}{30} + \frac{Mn + Cr + Cu}{20} + \frac{Ni}{60} + \frac{Mo}{15} + \frac{V}{10} + 5B.$

Adding of nitrogen (0.02–0.03 %), nitride-forming and microalloying elements into the composition of these steels decreases the tendency to the growth of an austenitic grain in HAZ metal. Taking into account that the metal structure of separate regions of this zone is non-homogeneous, and their sizes are rather small, the samples-simulators of 13 × 13 × 150 mm, heat-treated in accordance with different thermal cycles of welding in installation MSR-75, were used [6]. During investigations the samples were heated to the temperature 1350 °C, and the cooling rate was changed within the range of $w_{6/5}$ = 2.7–35 °C/s. Specimens for static tensile strength (in the range of 20–800 °C) were manufactured from plates subjected to the effect of simulated thermal cycle of welding.

The carried out investigations prove the essential increase in strength of HAZ metal of the steels investigated (Figure 1) stipulated by the effect of thermal processes proceeding in it. Depending on the composition of a definite steel HAZ metal yield strength can be 1.03–1.35 times higher than in parent metal at delayed rates of cooling ($w_{6/5}$ = 2.7 °C/s) and 1.2–1.56 times higher at intensive rates ($w_{6/5}$ ≈ ≈ 36 °C/s).

As is known, the schematic diagrams of dependence of yield strength on temperature are usually used in approximate calculations of low-carbon steels. In alloyed steels this characteristic is defined as a conditional value by residual plastic deformation 0.2 %. Results of high-temperature investigations of mechanical properties (strength and ductility) of

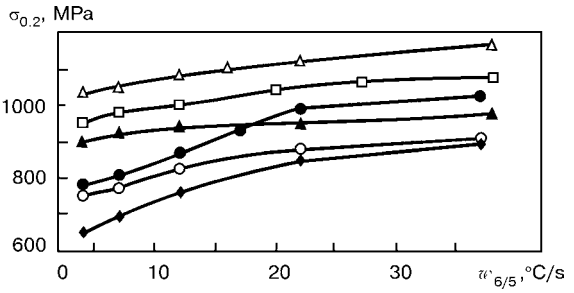

Figure 1. Effect of cooling rate on yield strength of HAZ metal of samples-simulators: ◆ – 12GN2MFAYu; ○ – 14KhG2SAFD; ● – 12GN3MFAYuDR; Δ – 14KhGN2MDAFB; ▲ – 12KhGN2MFBDAYu; ❒ – 12KhGN2MFDRA steel

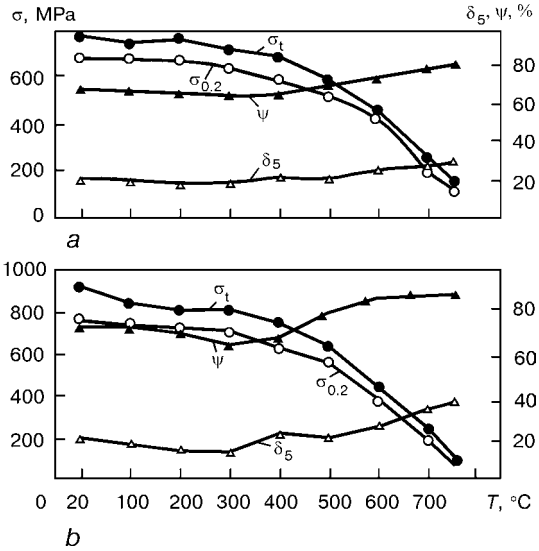

Figure 2. Mechanical properties of steel 12GN2MFAYu (*a*) and 14KhGN2MDAFB (*b*) at change in test temperature

high-strength steels are given in Figure 2. At temperature 750 °C the yield strength of steels 12GN2MFAYu and 14KhGN2MDAFB is about 50–100 MPa. With decrease in temperature approximately to 600 °C it increases and reaches the level of 60–65 % $\sigma_{0.2}$ (determined at temperature +20 °C). This regularity is preserved also in metal of simulated HAZ of high-strength steels (Figure 3).

The generalized information about the effect of test temperature on change in strength of the investigated steels and HAZ metal is given in Figure 4. Unlike the known diagram σ–ε it gives not the yield strength of parent metal σ_y in axis of ordinate, but the ratio of values of conditional yield strength of metal at definite increased temperature σ_{temp} to its conditional yield strength at temperature +20 °C $\sigma_{0.2}$. In the given case this approach was stipulated by the absence of a clearly expressed area of yielding in the tensile diagram of steels being investigated. More-

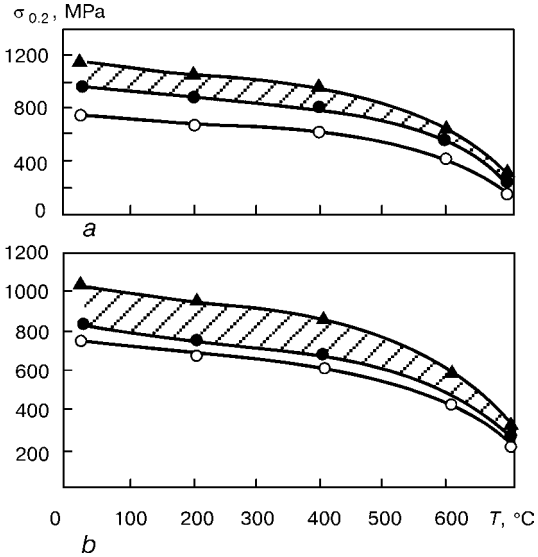

Figure 3. Effect of test temperature on yield strength of parent metal (○) and HAZ of joints at cooling rates $w_{6/5}$ = 2.7 (●) and 36 °C/s (▲): *a* – 14KhGN2MDAFB; *b* – 12GN3MFAYuDR steel

over, it was assumed that at $T \approx 780$–800 °C $\sigma_{0.2} = 0$ in the investigated areas of the welded joints. By the moment when the metal reaches 600–400 °C temperature the formation of high level of temporary tensile stresses is possible in welded joints. The value of these stresses depends on composition of steels and specifics of their cooling. However, at these temperatures the structural transformations are beginning to occur accompanied by increase in its volume, thus leading to the compression of adjacent regions of the welded joints. Deformations were determined from the results of processing of appropriate dilatometric curves. Dilatometric examinations provided heating of samples from the above-mentioned materials up to 1350 °C temperature at the rate of 150 °C/s, and then their cooling at the rates corresponding to different thermal cycles of welding (Figure 5). This enables us to reproduce the processes proceeding in alloy steels during formation of structure of the welded joints.

Cooling of alloy metal is accompanied by decrease in its volume. Process of deforming is complicated at $\gamma \rightarrow \alpha$ transformations, as the latter lead to the increase in volume of a crystalline lattice in the range of temperatures of phase transformations. The final result of the mentioned processes is defined by a definite metal composition, and also by peculiarities of proceeding and range of temperatures of phase transformations. In the given case the dilatometer sensors recorded the change in length ΔL of the samples investigated at a preset base L of investigations, that allowed us to calculate the relative deformation for each definite variant:

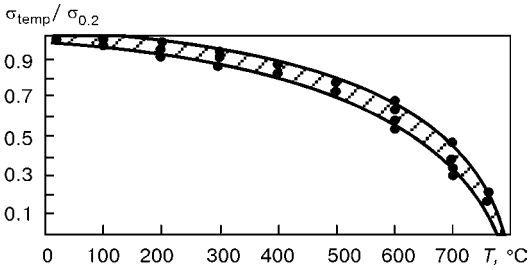

Figure 4. Effect of test temperature on change in strength of alloy structural steels

$$\varepsilon = \frac{\Delta L}{L} 100\ \%.$$

Using the dilatometric curves the relative deformation was calculated on straight regions each 50 °C, while on regions which are accompanied by structural transformations it was calculated each 5–10 °C. Point of beginning of sample heating was assumed to be equal to 0 in graphs. Dilatograms were processed in accordance with the procedure given in [7].

In steels investigated structural transformations are finished, as a rule, at temperatures (T_f, °C) below 300 °C and lead (Figure 6) to rather large deformations ε_c. The generalized data about the phase-structural changes of low-alloy steels are given in Table 2. All they refer to the range of cooling rates $w_{6/5} \approx$ $\approx$ 5–36 °C/s, which are most typical of arc welding of alloy steels. It follows from given data that a general law is preserved for all the steels investigated: the increase in structural compression deformations in HAZ metal at high rates of cooling (limited heat input of welding). Probably, the final level of residual stresses in HAZ metal of these steels is influenced by

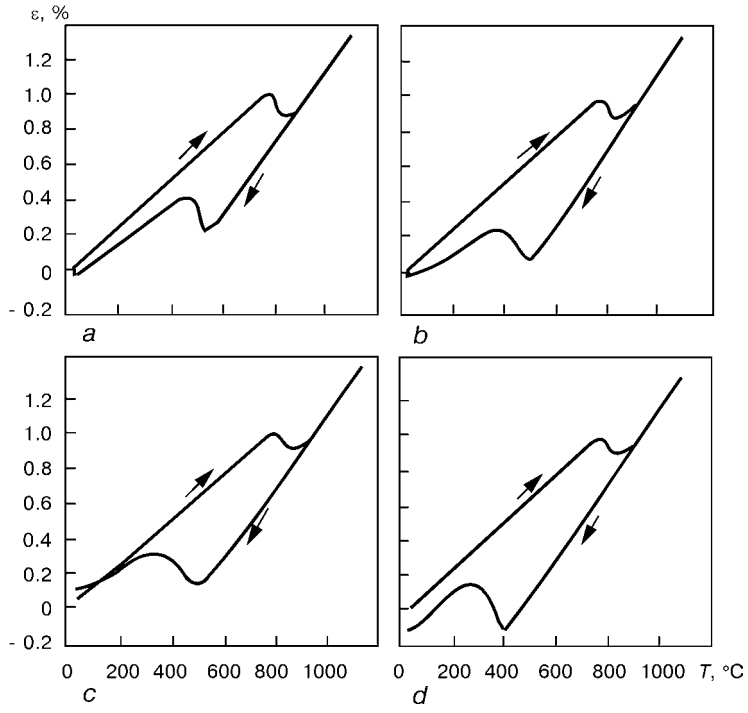

Figure 5. Dilatometric curves of heating-cooling of samples of steel 14KhG2SAFD at different rates of cooling: *a* — $w_{6/5}$ = 5; *b* — 8.5; *c* — 14; *d* — 36 °C/s

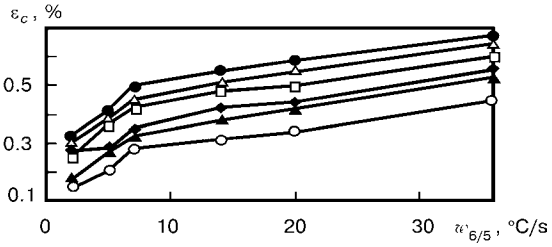

Figure 6. Effect of cooling rate on value of deformation in metal of HAZ of alloyed steels stipulated by the proceeding of structural transformations in them (see designations in Figure 1)

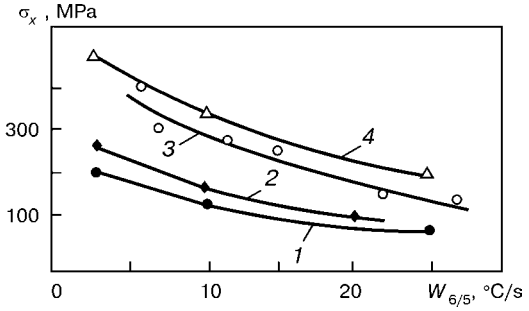

Figure 7. Effect of cooling rate on change in residual welding stresses σ_x in HAZ metal of steels 12GN3MFAYuDR (*1*), 12GN2MFAYu (*2*), 14KhG2SAFD (*3*) and 14KhGN2MDAFB (*4*)

the peculiarities of proceeding temperature and structural deformations of the metal being welded. This is proved by the results of comparative analysis of steels of 12GN3MFAYuDR and 14KhGN2MDAFB grades (Figure 3). The change in strength of HAZ metal under the influence of welding thermal cycle occurs in different ways. In 12GN3MFAYuDR steel it is 1.03–1.3 times increased as compared to that of the parent metal, while in 14KhGN2MDAFB it is 1.36–1.56 times increased.

At the same time at comparable rates of cooling the higher level of compression deformations caused by structural transformations can be formed in HAZ metal of 12GN3MFAYuDR steel. This gives grounds to assume that in welded joints of this steel the level of residual welding stresses will be lower. As compared with steel 14KhGN2MDAFB it is not alloyed with chromium and has the lower content of carbon and vanadium at almost equal amounts of manganese and molybdenum. All these elements contribute to a great extent to the increase in strength of HAZ metal of structural steels and improvement of characteristic of weldability P_{cm}, that characterizes the reduction of its resistance to a delayed fracture.

Similar observations are connected with one more pair of steels (12GN2MFAYu and 14KhG2SAFD), which also have the equal characteristics of strength, but they are differed by alloying. In this case steel 12GN2MFAYu is more preferable from the point of view of formation of residual welding stresses.

Thus, as a result of interaction of temperature and structural deformations the residual tensile stresses will be formed in HAZ metal of alloy structural steels. Results of the investigations carried out can be interpreted as regards to the conditions of fulfillment of a single-pass hardfacing on a massive plate. Formation of stresses in butt joints occurs to be more complicated and depends, as a rule, on many factors, such as design of joints and their rigidity, value of linear energy input, scheme of filling of edge groove, number of layers and beads in weld and others [7].

This was proved by investigations of HAZ metal produced in fulfillment of a single-pass hardfacing on a massive plate and welding of rigidly fixed butt joints with multipass welds. To fulfill the single-layer deposits by the automatic submerged arc and manual electric arc welding, the $400 \times 300 \times 30$ mm plates of steels 12GN2MFAYu, 14KhG2SAFD, 12GN3MFAYuDR and 14KhGN2MDAFB were used. During investigations the welding conditions and preheating temperature were controlled that made it possible to change the rate of cooling the HAZ metal within the interval $w_{6/5}$ = 7–27 °C/s. After this, the longitudinal residual stresses in these samples were determined using the method of holographic interferometry, developed at the E.O. Paton Electric Welding Institute [8]. As a rule, they are formed non-uniformly in length: their minimum levels are located at the beginning and end parts, while maximum levels are located in the middle part. Averaged values of residual stresses in HAZ metal of steels investigated depending on the rate of their cooling are given in Figure 7. The data obtained prove that the above-considered steels can be quite conditionally divided into two groups. The first group will include steels 12GN2MFAYu and 12GN3MFAYuDR, in which a relatively low level of residual stresses ($\sigma_x < 260$ MPa) is formed even in welding at increased heat inputs.

The second group includes the rest steels (14KhG2SAFD, 14KhGN2MDAFB, 12KhGN2MFBDAYu and 12KhGN2MFDRA), in which a high enough level of longitudinal residual tensile stresses ($\sigma_x \approx 350$–450 MPa) can be formed at delayed rates of cooling ($w_{6/5} < 5$ °C/s) as a result

Table 2. Characteristics of phase-structural transformations of high-strength alloy steels

Steel grade	T_b, °C	T_f, °C	ε_C, %	*Components of microstructure*
12GN2MFAYu	620–515	420–270	0.26–0.61	Bainite, martensite
14KhG2SAFD	575–411	318–232	0.14–0.47	Ferrite, bainite, martensite
12GN3MFAYuDR	510–404	228–203	0.33–0.68	Bainite, martensite
14KhGN2MDAFB	531–445	336–300	0.30–0.65	Same
12KhGN2MFBDAYu	484–416	305–253	0.18–0.53	»
12KhGN2MFDRA	480–450	269–239	0.24–0.60	»

of using high heat inputs. With increase in cooling rate the total level of residual stresses in HAZ metal of these steels can decrease.

To manufacture technological samples, steels of 12GN3MFAYuDR and 14KhGN2MDAFB grades with a rather close level of service properties were used. Technological sample, selected as a base of investigations, represented a plate of 400 × 400 × × 40 mm size, on which the plates of the steel investigated were mounted and welded around the entire perimeter (with a fillet welds of 10–12 mm leg). Here, a butt joint with V-shaped edge preparation (100 × × 300 × 15 mm sizes) was formed. Welding of samples was performed with a 1.2 mm dia. solid wire of Sv-10KhN2GSMFTYu grade in mixture of gases on argon base (Ar + 20 % CO_2) at the following conditions: I_w = 130–140 A, U_a = 22–24 V, v_w = 13–14 m/h. Fulfillment of each next layer of weld after a root bead was started after cooling the welded joint to 20–30 °C temperature. At such conditions of welding the rate of HAZ metal cooling in the range of 600–500 °C was 26–28 °C/s. Content of diffusive hydrogen $[H]_{diff}$ in all the cases remained unchanged and was equal to 3–4 ml per 100 g of deposited metal. Its concentration was determined by chromotographic method.

Residual stresses in the investigated samples were also determined by the method of holographic interferometry. Their levels in HAZ metal of joints made from steels 12GN3MFAYuDR and 14KhGN2MDAFB are given in Figure 8. The data obtained prove that the selected design and sizes of samples contribute to the formation of a high level and specific distribution of residual stresses in welded joints both along and across the weld axis. Thus, in welded joints of steel 14KhGN2MDAFB the value of stresses is 350–580 MPa. They are equal approximately to (0.5–0.8) $\sigma_{0.2}$ of the parent metal. The level of residual stresses is much lower at similar conditions of welding in joints of steel 12GN3MFAYuDR, it is 240–310 MPa. In the welded joint they are distributed almost uniformly, and their level does not exceed 45 % of the steel yield strength. This circumstance proves that the initiation and propagation of cold cracks are hardly probable in these joints. Similar regularities in formation and distribution of longitudinal and transverse stresses were also obtained in investigation of joints of steels of 12GN2MFAYu and 14KhG2SAFD grades. In the first grade they are much lower. It should be noted that the results of the carried out investigations are confirmed by a large experience in use of the above-mentioned steels [9, 10]. It was almost always possible to prevent the inition of cold

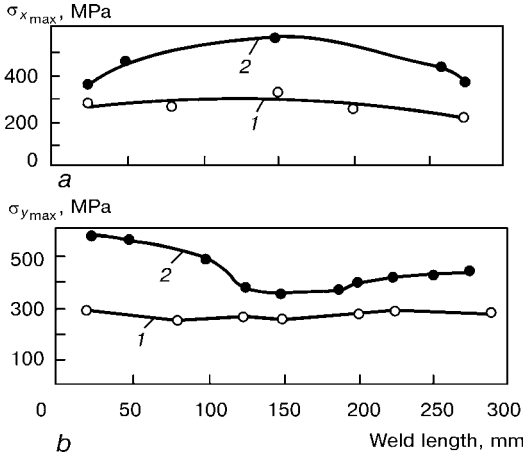

Figure 8. Residual longitudinal σ_x (*a*) and transverse σ_y (*b*) stresses in HAZ metal of technological samples of steels 12GN3MFAYuDR (*1*) and 14KhGN2MDAFB (*2*)

cracks in the welded joints in manufacture of unique critical structures from steels of 12GN2MFAYu and 12GN3MFAYuDR grades keeping the definite technological recommendations. This is due greatly to the formation of a relatively low level of residual stresses.

Results of investigations show that the rational use of the methods of investigation of weldability makes it possible to obtain the approximate information about the level of residual stresses in joints of alloy steels, to classify them by this characteristic and to select the most acceptable compositions of metals for manufacture of critical welded structures.

1. Lobanov, L.M., Pivtorak, V.A. (1992) Methods of investigation and control of welding stresses and strains. In: *Improvement of welded metal structures*. Kyiv: Naukova Dumka.
2. Makhnenko, V.I. (1998) Computer modelling of welding processes. In: *Advanced materials science of the 21st century*. Kyiv: Naukova Dumka.
3. Gladshtejn, L.I., Litvinenko, D.A. (1972) *High-strength structural steel*. Moscow: Metallurgiya.
4. Nikitin, V.N. (1977) High-strength low-alloy steels for automotive, excavating and mining engineering. *Stal*, **11**, 1044–1047.
5. Gladshtejn, L.I., Bobyleva, L.A., Onuchin, L.G. et al. (1978) Investigations and development of new high-strength steel for welded structures. *Ibid.*, **6**, 548–551.
6. Sarzhevsky, V.A., Sazonov, V.Ya. (1981) System for simulation of welding thermal cycles on the base of MSR-75 machine. *Avtomatich. Svarka*, **5**, 69–70.
7. Lobanov, L.M., Mikhoduj, L.I., Vasiliev, V.G. et al. (1999) Peculiarities of behaviour of thermodeformational processes in arc welding of high-strength steels. *Ibid.*, **3**, 3–11.
8. Lobanov, L.M., Pivtorak, V.A. (2000) Development of holographic interferometry for investigation of the stress-strain state and quality control of welded structures. *IIW Doc. XV-1036–00*.
9. Musiyachenko, V.F., Kasatkin, B.S., Mikhoduj, L.I. et al. (1982) Welding of high-strength steel 12GN2MFAYu. *Avtomatich. Svarka*, **5**, 47–50.
10. Mikhoduj, L.I., Yushchenko, A.K., Poznyakov, V.D. et al. (1991) Weldability of high-strength steel 12GN3MFAYuDRSSh. *Ibid.*, **11**, 12–16.

STRUCTURE AND PROPERTIES OF THE METAL DEPOSITED UNDER THE WATER BY FLUX-CORED WIRE WITH A NICKEL SHEATH

S.Yu. MAKSIMOV[1], **I.M. SAVICH**[1], **S.M. ZAKHAROV**[2], **N.V. ZAJTSEVA**[2] and **E.V. KOZLOV**[2]
[1]E.O. Paton Electric Welding Institute, NASU, Kyiv, Ukraine
[2]G.V. Kurdyumov Institute of Metal Physics, NASU, Kyiv, Ukraine

The paper anlyses the influence of the environment on gas content and density of a high-nickel (60–70 % Ni) weld metal, structure and properties of different zones of the welded joint. In order to improve the indices of their mechanical properties, the alloying, modifying and surface-active elements should be further added to the charge of the flux-cored wire.

Key words: *underwater welding, flux-cored wire, deposited metal, HAZ, gas content, structure, mechanical properties*

Welding has an important role in construction and repair of underwater pipelines. Wet welding has been widely used for these purposes recently. It is performed directly in the water environment and eliminates application of expensive caissons or chambers. However, use of earlier developed consumables in welding of the modern pipe steels of X60 type [1] yields negative results, as cold cracks are observed in the HAZ. This problem may be solved by applying electrode materials, which ensure formation of the austenitic structure of weld metal [2] and, thus, reduce the content of hydrogen, diffusing into the HAZ metal. Investigation of samples, welded with electrodes with a stainless steel rod, revealed a number of disadvantages [3–5]. Cracks may initiate in the fusion zone at solidification, because of the difference in the values of the coefficient of thermal linear expansion of the weld metal and the base metal. Moreover, mixing of the metal of the first pass with the base metal near the fusion boundary results in the appearance of a brittle martensite interlayer, prone to cold cracking.

Therefore, in this case, application of nickel electrodes is more promising [4–6]. The weld metal and the base metal have close values of the coefficient of linear thermal expansion, and presence of a great austenization margin allows avoiding formation of martensite interlayers. And although the metal of such welds is prone to formation of pores and hot cracks, particularly in the root pass, the welded joints made with nickel electrodes, had high resistance to cold cracking.

Application at PWI of flux-cored wires with rutile-based charge and steel strip sheath did not allow making welded joints of X60 type steel without cracks in the HAZ. It was not possible to achieve a high content of nickel in the weld metal by alloying the wire core.

Application of nickel strip is more rational. Since such wires were not used earlier, the purpose of this work was obtaining preliminary data on the possibility of formation of a sound deposited metal, and assessment of its structure and properties, also in the HAZ, in welding with a flux-cored wire with a nickel sheath. The experimental flux-cored wire charge was based on fluorides of alkali and alkali-earth metals, manganese metal being the de-oxidizer. Nickel strip of 0.3×8.0 mm size was used as the sheath. Deposition on a plate of X60 steel 14 mm thick was performed in the following mode: $I_w = 160–180$ A; $U_a = 32–34$ V; $v_w = 6$ m/h; reverse polarity current; wire diameter 1.8 mm; filling factor 26–28 %. Methods of durometry, optical and scanning electron microscopy, gas analysis [7], volumetry [8] and X-ray fluorescence analysis (XFA) were used in investigations. For convenience of studies, three zones were singled out in investigations, namely deposits, partially-melted regions and HAZ, which markedly differed from each other.

Figure 1 shows the microstructures of the above zones with reference to the macrostructure. As is seen from Figure 1, macrostructure of the deposited weld metal contains clearly defined regions of comparatively small equiaxed crystallites located along its boundaries, columnar crystals elongated along the direction of heat removal, and coarse-grained nugget, which is where metal solidification is completed.

Composition of metal, deposited under the water, is given in Table 1. Its comparison with the composition of the metal, deposited by the same wire in air, reveals an increased content of iron. Apparently, arc constriction and presence of turbulent gas flows in the vapour-gas bubble in underwater welding lead to a greater degree of mixing with the base metal and higher arc penetrability. The latter is confirmed by 15–20 % increase in the penetration depth in underwater welding, compared to welding in air. This results in an increase of the proportion of the base metal in the molten metal. In keeping with the diagram of phase equilibrium [9], a two-phase condition should

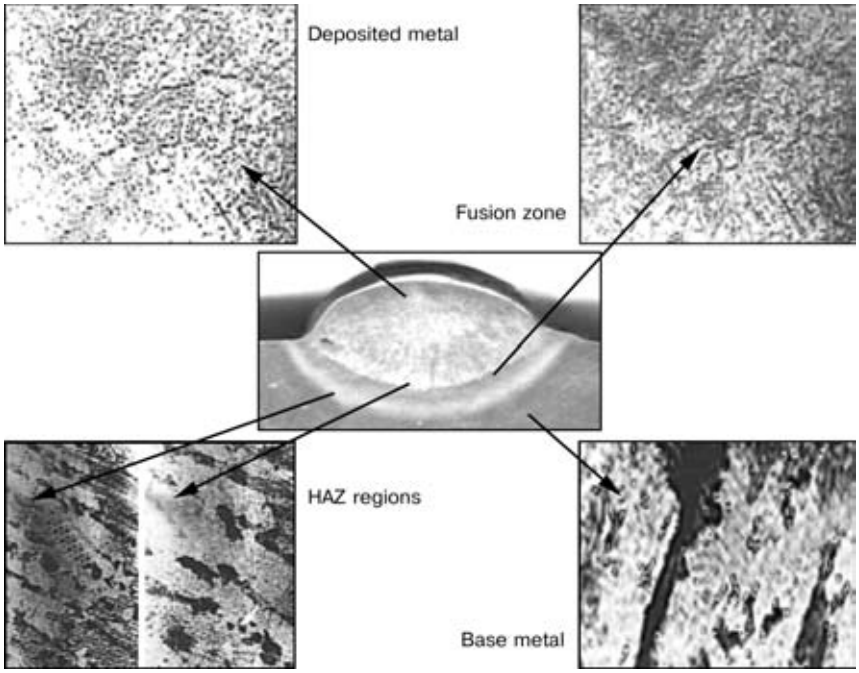

Figure 1. Microstructure of different regions of the deposit (*macrosection in the center*) on steel X60, made under the water with flux-cored wire with a nickel sheath (×309)

correspond to such a composition. This structure consists predominantly of solid solution of iron in nickel and ordered $FeNi_3$ phase. The second phase, however, was not revealed in the studied sample, either by metallographic or X-ray method. Apparently, the solidification conditions are such that instead of the equilibrium structures, a metastable structure is formed, which is an oversaturated solid solution of iron in nickel, or a disordered intermetallic [10, 11].

The width of the zone of a variable composition near the fusion boundary (Figure 2) is small enough (about 40 μm), and it does not have any interlayers with the hardening structure.

Microstructure of HAZ samples, made in air and under the water, differs only slightly. HAZ boundary is determined by the position of the isotherm, giving the direct ($\alpha \rightarrow \gamma$) and reverse ($\gamma \rightarrow \alpha$) phase transformations. In underwater welding the geometrical dimensions of the HAZ are reduced almost 3 times due to intensive cooling. HAZ metal undergoes a certain degradation of the initial lineage structure of the rolled steel. At heating in the region of γ-transformations partial dissolution of cementite of the eutectoid colonies in austenite occurs, and at subsequent cooling eutectoid colonies form again, their morphology and location differing from the initial ones. Degradation of the initial lineage structure in the rolled steel HAZ is more pronounced in underwater welding. This is due to a high rate of metal cooling, v, the values of which are higher than those required for formation of a layer structure [12]:

$$v \leq D_C \Delta T / \alpha^2, \qquad (1)$$

where D_C is the coefficient of carbon diffusion; ΔT is the difference of temperatures of $\gamma \rightarrow \alpha$ transformation in local regions of the material; α is the distance between the layers of pearlite colonies.

Welding conditions have the most dramatic influence on the microstructure of the fusion zone. In the case of welding in air it is practically not revealed separately from the HAZ, and is a section of the most dispersed ferrite-pearlite structure, characteristic for the entire HAZ. Water cooling changes the situation, leading to formation of finely-dispersed hardening structures (see Figure 1). In this case cracks in the deposited metal and HAZ are absent.

Butt joints were made on 14 mm X60 steel to determine the mechanical properties of the weld me-

Table 1. Composition of the deposited metal produced under different conditions of welding (by XFA data)

Welding conditions	*Fraction of elements, wt.%*			
	Fe	*Ni*	*Cr*	*Mn*
In air	23.90	73.14	0.01	2.85
Under the water	36.12	61.03	0.02	2.82

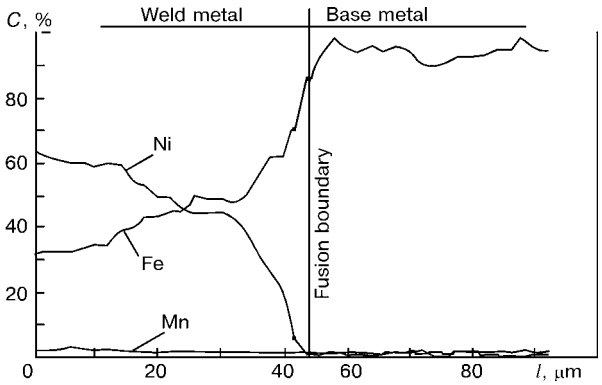

Figure 2. Element distribution near the fusion boundary in underwater welding by the data of X-ray microanalysis (C — element content; l — distance)

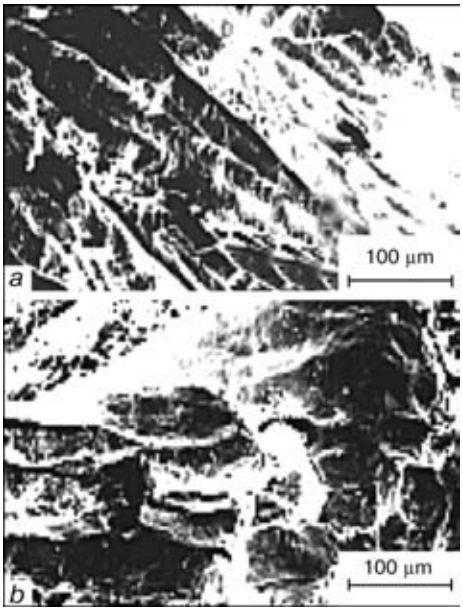

Figure 3. Fractograms of the sample fracture surface: *a* — central region of the deposited metal; *b* — its peripheral region

tal. However, it was not possible to obtain a sound weld metal suitable for testing, because of slag inclusions between the passes and near the edges being welded, which was caused by the use of fluoride slag. Therefore, for investigation purposes, a three-layer deposit into a groove was made, which was followed by preparation of samples of type II (to GOST 6996–66). Testing results showed that the deposited metal is characterized by a low level of mechanical properties ($\sigma_t \le 290$ MPa, $\delta \le 6$ %). This is caused by the presence of a coarse-crystalline structure in the coarse-grained nugget in combination with precipitation of nickel oxide and hydrogen along the grain boundaries. Intensive heat removal from the deposited metal regions, adjacent to the surface and the fusion boundary, leads to formation of a comparatively fine-crystalline structure. Therefore, fractographic studies of the fracture surface of samples after tensile testing showed that this process is of a mixed mode (Figure 3): brittle in the central region in the site of crack initiation and tough-brittle at subsequent propagation of the crack into the peripheral regions of the deposited metal [13].

Durometric studies permitted determination of the mechanical properties of local regions of the deposited metal (deposited metal with a fine-grained structure, adjacent to the fusion boundary), fusion zone and HAZ. Obtained results (Table 2) demonstrate the inhomogeneity of its structure and influence of the environment. Deposited metal enrichment in iron from the base metal (see Table 1) and accelerated cooling lead to a higher hardness and strength in samples welded under the water.

For materials with non-uniform properties it is rather difficult to evaluate the ductile properties in the local regions. Therefore, of considerable interest are the evaluations produced by the method of durometry [14, 15]. In this case the following relationship is used as the ductility parameter δ_n:

$$\delta_n = 1 - \frac{\varepsilon_e}{\varepsilon}, \qquad (2)$$

where ε_e is the elastic deformation; $\varepsilon \approx 0.076$ is the total deformation on the indentor–sample contact area in the direction of the tensile force application. Elastic deformation ε_e is defined from the following formula:

$$\varepsilon_e = 1.08\,(1 - \nu - 2\nu^2)\,\frac{HV}{E}, \qquad (3)$$

where ν is the Poisson's ratio; HV is the Vicker's hardness; E is the Young's modulus. Values of δ_n calculated for a large number of materials reflect the concepts of their ductility formed on the basis of standard mechanical tests. It is found that the critical value of ductility is equal to $\delta_n \ge 0.9$. Achievement of this value is the mandatory condition for ductility manifestation in tensile and bend testing of materials.

Measurements showed that in underwater welding the deposited metal with the fine-grained structure in the fusion zone, as well as in the local regions in the HAZ has a sufficiently high ductility margin, as in all the studied zones $\delta_n > 0.9$, which is higher than the critical value [15]. On the other hand, δ_n values in the fusion zone and the HAZ are below similar values for the base metal. Ductility of the deposited metal, even though it is lower than in welding in air, is still higher than that of the base metal.

The environment, in which welding is performed, also has a marked influence on the density of the deposited metal and its gas content (Table 3). In this case the content of gases and the density do not correlate.

In welding under the water deposited metal of a high density is produced, which was not obvious a priori. It should be noted that metallographic examination did not reveal any noticeable porosity in the deposited metal, despite the lower density compared to the base metal, which was determined by hydrostatic weighing. It is known [16] that being an active

Table 2. Mechanical properties of the metal deposited (in air and under the water) on X60 steel

Welding conditions	*Hardness* HV_{100}, *GPa*				*Yield point* $\sigma_{0.2}$, *GPa*				*Ductility parameter* δ_n, *%*			
	DM	*FZ*	*HAZ*	*BM*	*DM*	*FZ*	*HAZ*	*BM*	*DM*	*FZ*	*HAZ*	*BM*
In air	1.120	1.58	1.61	1.60	37.3	52.5	53.5	53.2	0.959	0.938	0.937	0.937
Under the water	1.415	2.16	2.03	1.60	47.2	72.0	67.7	53.2	0.948	0.914	0.910	0.937

Note. DM — deposited metal; FZ — fusion zone; BM — base metal.

Table 3. Density of the deposited metal and its content of gases under different conditions of welding

Welding conditions	*Density of deposited metal, g/cm³*		*Change of density*		*Gas content S·10⁻², wt.%*	
	measured ρ_m	*calculated* ρ_c	$\Delta\rho = \rho_c - \rho_m$, *g/cm³*	$\Delta\rho/\rho_c$, %	*[O]*	*[H]*
In air	8.27691	8.4999	0.22298	2.623	2.00	0.16
Under the water	8.37890	8.5711	0.19220	2.242	0.71	0.36

element, oxygen forms the following chemical compound with nickel:

$$O + Ni \leftrightarrow NiO.$$

Hydrogen, evolving from nickel simultaneously with oxygen, reduces nickel oxide in view of lowering of the solubility:

$$NiO + 2H \leftrightarrow Ni + H_2O.$$

When this reaction proceeds in the weld pool, evolution of water vapours results in an intensive boiling of liquid metal, and after solidification is over the weld metal usually contains pores. In the case of underwater welding a significant content of hydrogen in the vapour-gas channel leads to binding of a certain amount of oxygen, and the probability of nickel oxide formation in the molten metal is lower. Therefore, at the moment of the weld pool solidification the process of interaction of hydrogen and nickel oxide is of a limited nature, which reduces the probability of pore formation.

Thus, investigation results showed that application of flux-cored wire with a nickel strip sheath allowed producing a sufficiently dense deposited metal without cracks, coarse pores or non-metallic inclusions. The brittle mode of sample fracture in tensile testing is related to formation of a coarse-crystalline structure in the central part of weld. However, ductility of local regions of the deposited metal with a fine-grained structure has values above the critical ones. Considering that the flux-cored wire with a nickel sheath without any additional alloying of the charge was used for investigations solely as model material, the required properties and structure of the weld metal can be produced, using purpose-oriented alloying by adding modifiers and active deoxidizers to the flux-cored wire core. After this problem has been solved, further efforts will be aimed at evaluation of the welding-processing properties of the flux-cored wire and determination of the performance of the welded joint on X60 type steel as a whole.

1. Ibarra, S., Grubbs, C.E., Liu, S. (1995) State-of-the-art and practice of underwater wet welding of steel. In: *Proc. of Int. Workshop on Underwater Welding of Marine Structures*, December 7–9, 1994, New Orleans, Miami. New York: ABS.
2. Koibushi, M., Yokota, T. (1981) Underwater wet welding with Ni, Fe–Ni and stainless steel electrodes. *J. JWS*, **5**, 489–495.
3. Liu, S., Olson, D., Ibarra, S. (1991) Electrode formulation for underwater welding. In: *Proc. of Int. Conf. on Underwater Welding*, March 20–21, 1991, New Orleans, Miami. New Orleans: AWS.
4. Szelagowski, H., Stuhff, H., Loebel, P. (1989) Properties of wet welded joints. In: *Proc. of 21st Ann. OTC*, May 1–4, 1981, Houston.
5. Bailey, N. (1991) Welding under water — a metallurgical appraisal. In: *Proc. of 1st Int. Offshore and Polar Engineering Conf.*, August 11–16, 1991, Edinburg.
6. Gooch, T.G. (1983) Properties of underwater welds. Part 1. Procedural trials. *Metal Construction*, **3**, 164–167.
7. Pokhodnya, I.K. (1972) *Gases in welds*. Moscow: Mashinostroenie.
8. Gavrilyuk, V.G. (1977) Volumetric analysis. In: *Encyclopedia of inorganic materials*. Vol. 2. Kyiv: Ukr. Sov. Ents.
9. Hansen, M., Andreenko, K. (1962) *Structures of binary alloys*. Refer. Book. Moscow: Metallurgizdat.
10. Golubtsova, R.B. (1969) *Phase analysis of nickel alloys*. Moscow: Nauka.
11. Maltsev, M.V. (1970) *Metallography of industrial non-ferrous metals and alloys*. Moscow: Metallurgiya.
12. Martin, J., Doerti, R. (1978) *Stability of microstructure of metallic systems*. Moscow: Atomizdat.
13. Engel, L., Klinkele, G. (1986) *Scanning electron microscopy. Fracture*. Refer. Book. Moscow: Metallurgiya.
14. Markovets, M.P. (1979) *Determination of mechanical properties of metals by hardness*. Moscow: Mashinostroenie.
15. Milman, Yu.V., Galanov, B.A., Chugunova, S.I. (1992) *Characteristic of ductility, obtained in hardness measurement*. Kyiv: IPM.
16. Bagryansky, K.V., Kuzmin, G.S. (1983) *Welding of nickel and its alloys*. Moscow: Mashgiz.

EFFECT OF PLASMA-DETONATION TREATMENT OF SURFACE OF STEEL U8 ON THERMAL STATE AND PHASE COMPOSITION OF MODIFIED LAYERS

Yu.S. BORISOV and **O.V. KOLISNICHENKO**
E.O. Paton Electric Welding Institute, NASU, Kyiv, Ukraine

Temperature fields of surface layers during plasma-detonation treatment (PDT) of parts were determined through solving the non-stationary heat conduction equation by the finite difference method. The relationships derived were used for analysis of the kinetics of phase transformations in structure of steel U8 during PDT. The calculation-theoretical analysis results were compared with the experimental data.

Key words: *carbon steel, plasma-detonation treatment, finite difference method, non-stationary heat conduction equation, temperature fields, high-rate heating (cooling), structural-phase transformations*

The effect exerted by high-intensity heat flows formed by plasma generator, laser or electron beam leads to heating of the surface, followed by cooling through transfer of heat into a material and environment, thus resulting in structural-phase transformations occurring in the subsurface layer. High-rate heating and cooling cause changes in the kinetics of structural transformations, thus resulting in a shift of the corresponding critical phase transformation points [1, 2]. In the case of high-rate heating the heat input is higher than the energy required for restructuring of the crystalline lattice, $\alpha \rightarrow \gamma$, which occurs at a certain rate. In addition, homogenisation of austenite and the process of recrystallisation of deformed alloys shift to a range of even higher temperatures.

It is important to know the temperature field and a change in the heating (cooling) rate within the affected zone to determine shifts of temperatures of phase transformations occurring in steels under the influence of the concentrated energy source with respect to the critical points in the Fe–C equilibrium diagram. A large amount of studies were dedicated to mathematical modelling of the effect of the concentrated heat flows on materials [3–5]. They consider both analytical methods and methods of numerical analysis of thermal state of a material. In some studies modelling of the effect on the surface not by the stationary heat flow, but by the periodic one is performed.

The purpose of this work was to numerically calculate temperature fields and rates of their variations, as well as analyse their effect on the kinetics of phase transformations in modified layers during plasma-detonation treatment (PDT) of surfaces of parts. The PDT technology [6] allows formation of the pulsed plasma flows, under the effect of which the part surface undergoes cyclic heat treatment. The temperature range of heating of the surface is wide, i.e. from 20 to 2000 °C and higher. Therefore, in addition to variations in thermal-physical characteristics depending upon the temperature of a material treated, it is necessary to take into account also the latent heat of a phase transition. A distinctive feature of PDT is that a part can be included into the discharge circuit. Study of amplitude-time characteristics of the current in PDT showed that the current density in a region treated is above 10^8 A/m^2 [7]. Thus, heating of the surface layer of a material under the PDT conditions occurs due to an external heat flow, the components of which are as follows: energy transferred by electrons, ions and neutral atoms, radiant energy, and energy resulting from the heat released during passage of the pulsed current. Considering a wide temperature range of heating of the surface, it is necessary also to allow for variations in the electrophysical properties of a material. Therefore, it is more preferable to use numerical modelling of the process to calculate the dynamics of temperature fields during PDT. This was done by using the finite difference method. The fully implicit diagram was employed to solve the problem by this method.

The non-stationary heat conduction equation with variable coefficients and volumetric heat release was considered in an axisymmetric approximation:

$$C(T)\,\rho(T)\,\frac{\partial T}{\partial t} = \frac{\partial}{\partial z}\left[\lambda(T)\,\frac{\partial T}{\partial z}\right] + \frac{1}{r}\,\frac{\partial}{\partial r}\left[r\lambda(T)\,\frac{\partial T}{\partial r}\right] + \frac{j^2(t)}{\sigma(T)}, \quad (1)$$

$$0 \le r \le R, \quad 0 \le r \le H,$$

where C, λ, σ and ρ are the specific heat, thermal conductivity coefficient, specific electrical conductivity and material density, respectively; j is the current density determined experimentally using the Rogovsky zone method [7]; and R and H are the radius and thickness of a specimen, respectively.

Relationship between the surface and volumetric heat sources has the following form [8]:

$$\theta = \lambda T/(\chi\, j^2\, \delta^2),$$

where $\lambda = 20$ W/(m·K); $T = 1000$ K is the temperature in a layer; $\chi = 2 \cdot 10^{-6}$ Ohm·m is the specific electrical resistance; $j = 3 \cdot 10^8$ A/m^2; and $\delta = 10^{-4}$ m is the characteristic depth of the layer.

As shown by the estimation performed, volumetric heat release is 10 % of the total heat input. The following assumptions were made to formulate boundary conditions for equation (1): a part is heat insulated, specific heat flow into the part has a Gaussian distribution $q(r) = q_0 \exp[-(\xi r)^2]$ (q_0 is the maximum value of the specific heat flow and ξ is the coefficient allowing for variation of the specific heat flow along the radius), cooling of the surface is done due to heat transfer deep into metal, as well as due to a radiant flow from the part surface $q_r = \varepsilon\sigma_{SB}T^4$ (ε is the emissivity factor of the surface and σ_{SB} is the Stefan–Boltzmann constant):

$$z = 0, \quad 0 \le r \le R; \quad \lambda\frac{\partial T}{\partial z} = -q(r) + q_r;$$

$$z = H, \quad 0 \le r \le R; \quad \lambda\frac{\partial T}{\partial z} = 0;$$

$$r = 0, \quad 0 \le z \le H; \quad \frac{\partial T}{\partial r} = 0;$$

$$r = R, \quad 0 \le z \le H; \quad \lambda\frac{\partial T}{\partial r} = 0;$$

$$t = 0, \quad T = 293 \text{ K}.$$

To simplify the difference method, equation (1) was reduced to a quasi-linear form by the following substitution:

$$S(T) = \int_{273}^{T} \lambda(T)\mathrm{d}T.$$

Then equation (1) takes the following form:

$$\frac{C(T)}{\lambda(T)}\rho\frac{\partial S(T)}{\partial t} = \frac{\partial^2 S(T)}{\partial z^2} + \frac{1}{r}\frac{\partial}{\partial r}\left(\frac{\partial S(T)}{\partial r}\right) + \frac{j(t)^2}{\sigma(T)}. \quad (2)$$

The pulsed plasma effect results in a high temperature gradient formed in the surface layers. Therefore, the non-stationary heat conduction equation should be solved using a non-uniform grid, which makes the problem a bit more difficult. The following transform of coordinate z [9] was made to change to the uniform grid:

$$z = H\frac{1 - e^{\eta\tilde{z}}}{1 - e^{\eta}}, \quad (3)$$

where η is the coefficient allowing for the degree of non-uniformity of the grid;

$$\tilde{z} = \frac{\ln(1 - z(1 - e^{\eta})/H)}{\eta}$$

is the dimensionless coordinate on the uniform grid.

Allowing for transform (3), equation (2) on the uniform grid in a new coordinate system will have the following form:

$$\frac{C(T)}{\lambda(T)}\rho\frac{\partial S}{\partial t} = \frac{\partial^2 S}{\partial\tilde{z}^2}\frac{1}{\eta^2}\left(\frac{e^{\eta} - 1}{He^{\eta\tilde{z}}}\right)^2 - \frac{\partial S}{\partial\tilde{z}}\frac{1}{\eta}\left(\frac{e^{\eta} - 1}{He^{\eta\tilde{z}}}\right)^2 + \frac{1}{r}\frac{\partial}{\partial r}\left(\frac{\partial S(T)}{\partial r}\right) + \frac{j(t)^2}{\sigma(T)}. \quad (4)$$

Upon reduction to the dimensionless form, the difference analogue of equation (4) can be solved using the Pichman–Radford diagram [9] by the method of unidimensional runs along z and r.

The non-uniform time grid was used to ensure efficiency of the diagram and decrease pitches during cooling of the surface. The grid becomes denser in the time period of existence of high temperature gradients, and becomes looser at low gradients. The pitch of the grid can be determined from the following expression:

$$\tau = \frac{\tau_1(1 - \omega^k)}{1 - \omega}, \quad k = 0, 1, \ldots, l_c,$$

where l_c is the number of pitches in the calculation time grid during cooling; ω is the geometric progression coefficient describing non-uniformity of the grid on a time coordinate; and τ_1 is the first pitch in time during cooling.

Allowance for the phase transition heat in the calculation model was made by substituting the efficient heat capacity for the true one $C(T)$ in a temperature range of transition from one aggregate state to the other [10].

Numerical calculation of variations of temperature fields in surface layers of the U8 steel specimens was made for the following parameters of PDT: specific heat flow into the surface $q_0 = 7.2\cdot10^8$ W/m^2, pulse duration $\tau = 0.6$ ms, current amplitude $I = 5.0\cdot10^3$ A, specimen thickness $H = 5.0\cdot10^{-3}$ m, specimen radius $R = 5.0\cdot10^{-3}$ m, number of pulses $n = 6$, and pulse frequency $\nu = 3$ Hz.

During heating the critical point A_{c_1} shifts to a range of high temperatures by a value of ΔT_k [1]:

$$\Delta T_{cr} = \left(\frac{3k^2x^2}{4D}\right)^{1/3} v_h^{1/3}, \quad (5)$$

where D is the coefficient of diffusion of carbon in austenite; v_h is the heating rate in a critical temperature range; k is the parameter determined from the Fe–Fe$_3$C diagram ($k = 110$ for steel); x is the structural factor (half a distance between the neighbouring centres of solidification of austenite).

Figure 1 shows variations of temperature with time at points with coordinate $r = 0$ mm at a differing distance from surface z. The use of the Fe–C equilibrium diagram to determine thickness of the modified layer yields an overvalue of 60 μm. To determine thickness of the surface layer subjected to phase transformations under the PDT conditions, it is necessary to know the heating rate. Figure 2 shows the calculation curves for the heating rate at a differing depth. It can be seen that at $t = 6.0\cdot10^{-4}$ s and a depth of $z = 60$ μm the heating rate is $v_h \approx 1\cdot10^6$ K/s, and at a distance of $z \le 40$ μm from the surface $v_h \approx 1.5\cdot10^6$ K/s. For hardened steel U8 the structural factor is $x = 10^{-5}$ cm, and the coefficient of diffusion of carbon in austenite under the conditions considered is $D \approx (15–18)\cdot10^{-8}$ cm^2/s [1].

Based on equation (5), the critical point A_{c_1} shifts to a range of high temperatures by a value of $\Delta T_{cr} = 182–196$ °C. Thus, the non-isothermal austenitic

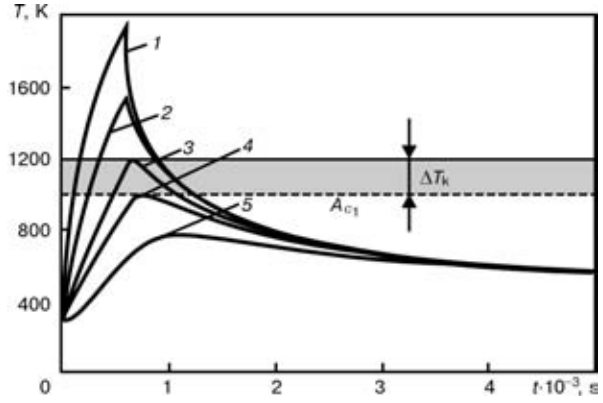

Figure 1. Temperature curves at points with coordinate r = 0 mm at depth: *1* — z = 0; *2* — 20; *3* — 40; *4* — 60; *5* — 100 μm

transformation ends at a temperature of about 1200 K. Therefore, the martensitic transformation (Figures 1 and 3) may occur in the surface layer at a depth of about 40 μm during subsequent cooling. Lying deeper is a structure formed at a high-temperature rapid tempering. Depending upon the cooling rate, the modified layer may comprise pearlite, sorbite, troostite, bainite and martensite.

The results obtained from electrothermic treatment of materials [2] show that the high-temperature decomposition of austenite can be fully suppressed at a cooling rate of 10000 K/s and higher, and only the martensitic transformation can be fixed at any stage of the pearlitic-austenitic transformation. Figure 4 shows the distribution of temperature through thickness of the modified layer at different moments of cooling. At $t = 1.0 \cdot 10^{-2}$ s the temperature of the surface layer is lower than the martensitic transformation temperature M_s = 518 K for steel of the U8 grade. At the given time moment the cooling rate is $v_c \approx$ ≈ 12000 K/s (Figure 5). Therefore, under the PDT conditions considered (according to the calculation-theoretical analysis results) the modified layer on the given steel will consist of the martensite and retained

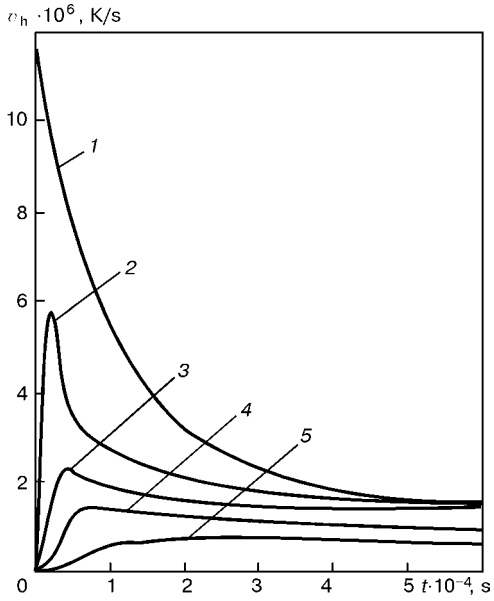

Figure 2. Heating rate at a distance from the surface: *1* — 0; *2* — 20; *3* — 40; *4* — 60; *5* — 100 μm

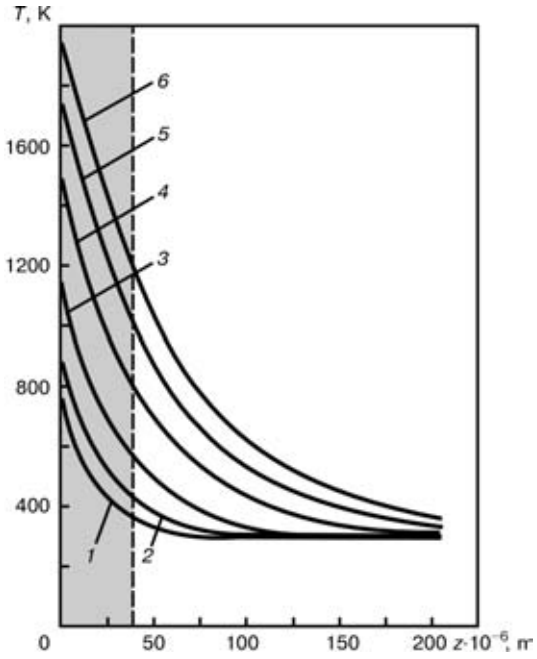

Figure 3. Distribution of temperature through thickness of the surface layer at r = 0 mm at the heating stage: *1* — $t = 4.5 \cdot 10^{-5}$; *2* — $7.5 \cdot 10^{-5}$; *3* — $1.5 \cdot 10^{-4}$; *4* — $3.0 \cdot 10^{-4}$; *5* — $4.5 \cdot 10^{-4}$; *6* — $6.0 \cdot 10^{-4}$ s

austenite phases. This is also proved by metallography of the modified layers of specimens subjected to PDT.

Figure 6 shows microstructure of the surface layer of a specimen from the given steel after PDT. X-ray phase analysis shows that the slightly etched white layer approximately 40 μm thick consists of a fine-crystalline martensite and retained austenite [11]. A high cooling rate leads to the fact that the resulting structure after cooling is highly heterogeneous, which is associated with heterogeneity of austenite formed during heating. In addition, this leads also to an increased imperfection of structure because of enhance-

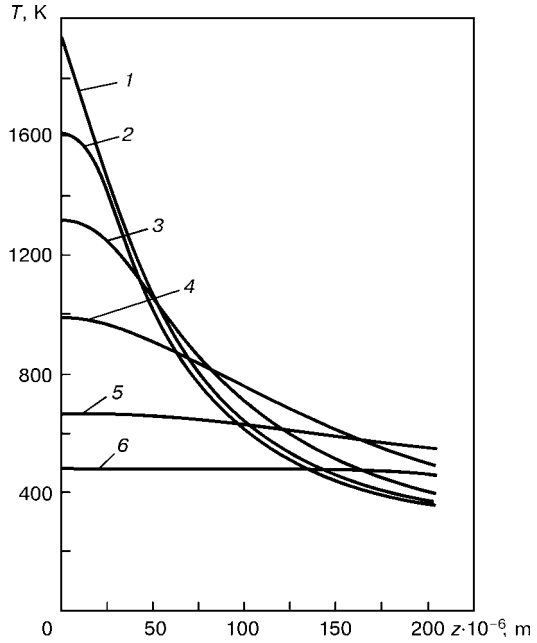

Figure 4. Distribution of temperature through thickness of the surface layer at r = 0 mm at the cooling stage: *1* — $t = 6.0 \cdot 10^{-4}$; *2* — $6.4 \cdot 10^{-4}$; *3* — $7.8 \cdot 10^{-4}$; *4* — $1.3 \cdot 10^{-3}$; *5* — $3.2 \cdot 10^{-3}$; *6* — $1.0 \cdot 10^{-2}$ s

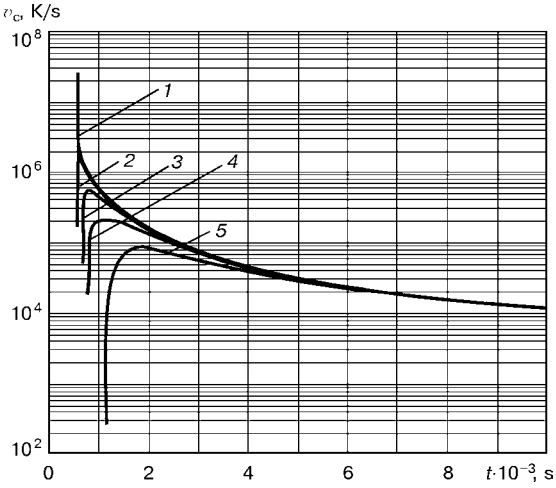

Figure 5. Cooling rate at depth: *1* — $z = 0$; *2* — 20; *3* — 40; *4* — 60; *5* — 100 μm

ment of phase hardening, slowing down of the relaxation and recrystallisation processes and a higher degree of inheritance of the γ-phase defects. This is accompanied by refining of blocks, increase in the dislocation density and growth of stresses in the crystalline lattice [12]. Martensite formed in this case is more dispersed than that formed in conventional hardening. In steel U8 after conventional hardening the length of the martensite needles is 7–10 μm, whereas after hardening using concentrated heat sources it is no more than 2–3 μm [12].

Based on the calculation curves (see Figure 3), the layer is penetrated to 5.5 μm. Also, it can be seen from Figure 5 that the cooling rate during solidification of the melt on the surface is higher than 10^6 K/s. In this case the dendritic growth of grain is degenerated to form the plane front of the grain [12]. Refining of grains has a favourable effect on properties of the alloy. And what is most important is that it is possible to achieve the optimal combination of strength and ductility. Refining of grains has the highest effect on increase in creep resistance, as the grain boundaries effectively hinder the plastic flow of metal at increased temperatures.

The above calculation curves apply to the effect of one pulse. Study of the effect exerted by the second and further pulses shows no substantial differences in the character of distribution of temperature fields. An intensive transfer of heat into metal takes place between the pulses. The surface layer has time to cool down to a temperature which differs to a negligible degree from the initial one. The temperature difference is no more than 10 °C. Therefore, PDT results in realisation of the process of thermal-cyclic treatment of the surface, leading to enhancement of phase hardening due to the reversible $\alpha \leftrightarrow \gamma$ transformations, increase in the dislocation density and decrease in the grain size, which is favourable for improvement of performance of parts. Widening of lines in X-ray patterns of the specimens subjected to PDT also evidences the presence of substantial phase hardening, resulting from the reversible $\alpha \leftrightarrow \gamma$ transformations during thermal cycling. Considering the shift of the critical points, the layer that undergoes hardening as a result of thermal cycling under the initial conditions studied is about 40 μm deep.

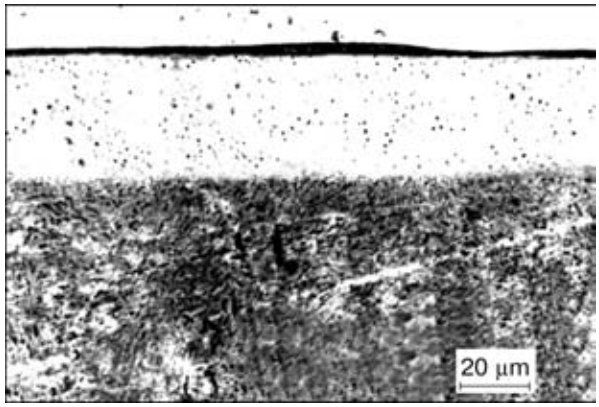

Figure 6. Microstructure of the U8 steel specimen after PDT

CONCLUSIONS

1. Heating of the surface of steel U8 under the PDT conditions leads to a shift of critical points A_{c_1} to a range of high temperatures by a value of ΔT_{cr} = 182–196 °C. Subsequent high-rate cooling results in a complete suppression of the high-temperature decomposition of austenite, causing only the martensitic transformation to occur. Under such conditions the modified layer consists of the martensite and retained austenite phases.

2. The multiple thermal effect during PDT allows realisation of the process of thermal cycling of the surface, promoting enhancement of phase hardening as a result of the reversible $\alpha \leftrightarrow \gamma$ transformations, increase in the dislocation density and refining of structure.

3. Estimates of thickness and phase composition of the modified layers are comparable with the data of experimental studies of the U8 steel specimens subjected to PDT. This enables the described calculation model to be used to predict kinetics of phase transformations and thickness of the modified layers under the PDT conditions for different grades of steels.

1. Gridnev, V.N., Meshkov, Yu.Ya., Oshkaderov, S.P. et al. (1973) *Physical principles of electrothermal strengthening of steel*. Kyiv: Naukova Dumka.
2. Kidin, I.N. (1969) *Physical principles of electrothermal treatment of metals and alloys*. Moscow: Metallurgiya.
3. Pereloma, V.A., Tarasevich, N.I., Liker, R.A. (1995) Investigation of thermal processes in laser treatment of iron-carbon alloys. *Protsessy Litia*, **2**, 38–48.
4. Uglov, A.A., Volkov, L.A., Sagdedinov, O.G. (1992) On construction of analytical solution for one-dimensional problem of metal fusion by a concentrated energy flow. *Inzh.-Fizich. Zhurnal*, **1**, 31–34.
5. Lykov, A.M., Naumenko, N.N. (1995) Fusion of materials by periodic heat flow. *Fizika i Khimiya Obrab. Materialov*, **2**, 107–115.
6. Tyurin, Yu.N., Kolisnichenko, O.V., Tsygankov, N.G. (2001) Pulse-plasma hardening of tools. *The Paton Welding J.*, **1**, 38–44.
7. Borisov, Yu.S., Kolisnichenko, O.V. (2000) Investigation of amplitude-time characteristics of the current pulse in plasma-detonation treatment of items. *Ibid.*, **12**, 55–59.
8. Gordeev, V.F., Pustogarov, A.V. (1988) *Thermionic arc cathodes*. Moscow: Energoatomizdat.
9. Anderson, D., Tannehill, J., Pletcher, R. (1990) *Computational hydromechanics and heat exchange*. Vol. 1. Moscow: Mir.
10. Grigoriants, A.G. (1989) *Principles of materials laser treatment*. Moscow: Mashinostroenie.
11. Borisov, Yu.S., Kolisnichenko, O.V. (2003) Effect of parameters of heating the surface of a part on structure of hardened layers of steel U8 in plasma-detonation treatment. *The Paton Welding J.*, **3**, 22–26.
12. Grigoriants, A.G., Safonov, A.N. (1987) *Laser technique and technology*. Book 3. Methods of surface laser treatment. Moscow: Mir.

PROCEDURE OF DETERMINATION OF SIZES OF ULTRADISPERSED NON-METALLIC INCLUSIONS IN METAL OF LOW-ALLOY STEEL WELDS

G.M. GRIGORENKO, V.F. GRABIN, V.V. GOLOVKO, V.A. KOSTIN, I.I. ALEKSEENKO and **L.M. KAPITANCHUK**
E.O. Paton Electric Welding Institute, NASU, Kyiv, Ukraine

The procedure envisages to use the numerical methods of obtaining images by scanning electron and light microscopes. The application of optical method of determination of sizes of inclusions using a digital camera gives an opportunity to determine inclusions which sizes exceed 0.07 μm.

Key words: *low-alloy steel, weld, non-metallic inclusions, structure, numerical image, electron microscopy*

A great interest is observed in scientific-technical literature of the recent years to the problems related to the conditions of formation of structural components in the weld metal. Investigations, carried out in this field, are directed to the comprehensive studies of conceptions about the mechanisms of origination, growth and developing both the structure itself and also the non-metallic inclusions (NMI), forming in the cast metal composition. These works require new approaches to the problems of procedure of conductance of quantitative determinations of ultradispersed components of structures (for example, NMI of 0.08–0.20 μm sizes) using optical and electron microscopes.

At present a metallographic method of determination of NMI sizes using a light microscope (LM) and automated units of «Quantimet», «Omnimet», «Epiquant» and other types is widely used. However, these units possess a relatively low resolution, i.e. it is possible to determine inclusions which size exceeds 0.27 μm (from the physical point of view it is minimum size of objects for examination in LM). This is due to the fact that the objects, which size is smaller than the length of light wave (λ = 270 nm), are not recorded. Here, the smaller particles are not taken into account, because many researchers associate their sizes with the formation of structure of acicular ferrite, providing optimum combination of strength and ductile properties of welded low-alloy welds.

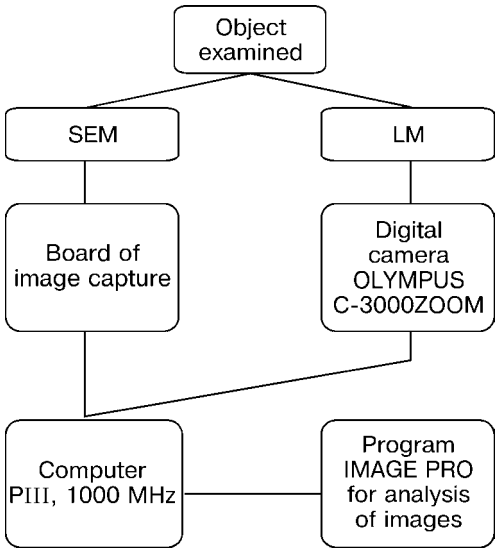

Figure 1. Schematic diagram of system of NMI analysis

Today, the numerical methods of producing images (for example, using digital or photographic cameras) find the wider spreading. Then, the numbered image is subjected to the analysis using an appropriate software. As a result a digital set of data containing a large volume of information is obtained, which can provide after analyzing the dimensional characteristics of the object examined.

In this connection the use of advanced means for revealing non-metallic particles of sizes of smaller than 0.5 μm is actual.

To analyze the NMI sizes, a scanning electron microscope (SEM) JEOL JSM-840 with a LINK SYSTEMS system of microanalyzers was used. The resolution of microscope is 40 nm, accelerating voltage — 5–35 kV, beam current — 10^{-7}–10^{-11} A. Examinations were carried out in the condition of secondary and back scattered electrons. LM «Neophot 32» with a digital camera OLYMPUS C-3000ZOOM was also used. The common matrix of image in it was 3340000 pixels. Maximum resolution of camera is 2048 × 1536 pixels. To have a quick control, a 1.8" colour LCD display is used. In the ZOOM condition the camera magnification is changed from 1 to 100 times. Figure 1 shows a schematic diagram of system for NMI analysis.

As an object of examinations, a section (polished, unetched) of weld metal on 14KhGNDTs steel, made by submerged arc welding, was selected. The section was preliminary subjected to ion cleaning for removing various contaminations from its surface. The obtained numerical image was transformed into double-coloured image using the program Image Pro, where the image of one colour corresponded to matrix, and that of another colour — to NMI (without distinguishing of their type). It should be noted that NMI

of different types are observed usually in the weld metal. As a consequence, the inclusions have a different level of grey colour in the numbered form. At this stage there were no task to classify the inclusions by types, however, it can be quite realizable. All the inclusions are referred conditionally to the same class, the level of upper and lower threshold of detection was set so that all they were analyzed. Data about the size and area of inclusions obtained using program Image Pro, were transferred to a written program to find the distribution of inclusions by sizes, construction of histograms and output of graphs for printing. To increase the validity of obtained results the analysis was performed in ten independent areas. Knowing the total area, where the inclusions were calculated, the volumetric share of NMI was also determined using SEM and LM. The results obtained are presented in Figure 2.

Comparing the results, obtained by SEM and LM, it was established that the volumetric share of NMI is in a good correlation with each other, i.e. 1.2 and 1.0 %, respectively. At the same time, some characteristic features are observed. Firstly, both methods show a very high content of the smallest inclusions up to 0.1 μm; secondly, the results obtained in SEM give a large number of fine inclusions, while the share of medium and large inclusions is increased in examination in LM; thirdly, the nature of curve of distribution of NMI using SEM and LM remains constant.

From analyzing the results obtained for NMI of sizes up to 0.1 μm an assumption was expressed that they include also the noise of electron microscope and digital camera, which were pre-detected as inclusions of sizes up to 0.1 μm. To separate the noise in detecting from ultradispersed inclusions, a following methodological approach was suggested. Sample of pure silver (99.99 %) was used for analyzing. Due to a high purity, the analyzed sample had not to have NMI, while any inclusions which would be detected were connected with electron noise of recording units. As a result, a threshold (0.07 μm) was established experimentally, at which the noise was not detected. Corrected results with allowance for removed noises are presented in the Table and in the form of histogram (Figure 3).

Thus, when the SEM is used, a large amount of highly-dispersed NMI within the 0.1–0.5 μm size are observed, while the data in the range of more than 0.5 μm, obtained in LM and SEM, are almost coincided. This circumstance is due to the higher resolution of SEM that leads to the feasibility of detecting finer NMI. Due to the fact that in LM examinations the comparatively small magnifications are used the total examined area in this case is much larger than the area examined in SEM, i.e. to obtain rather reliable results in determination of relatively large NMI, it is necessary to increase the number of fields examined in SEM.

To study the feasibility of determination of sizes of inclusions, smaller than 0.07 μm, similar examinations were made using SEM at 5000 times magnification. Analyzing the results obtained at high magnification we came to the conclusion that a shadow layer (locating between inclusion and matrix), whose formation is connected with the fact that the size of image pixel becomes comparable with inclusion size, begins to play an important role. Thus, if at ×1000 it was of order of 1–2 pixels, then at ×5000 it is comparable with a size of inclusions proper. Moreover, the smaller the particle size, the higher error in determination of size. Therefore, the volumetric share of inclusions determined at ×5000 can be changed noticeably within the ranges from 0.1 to 7–8 %, that

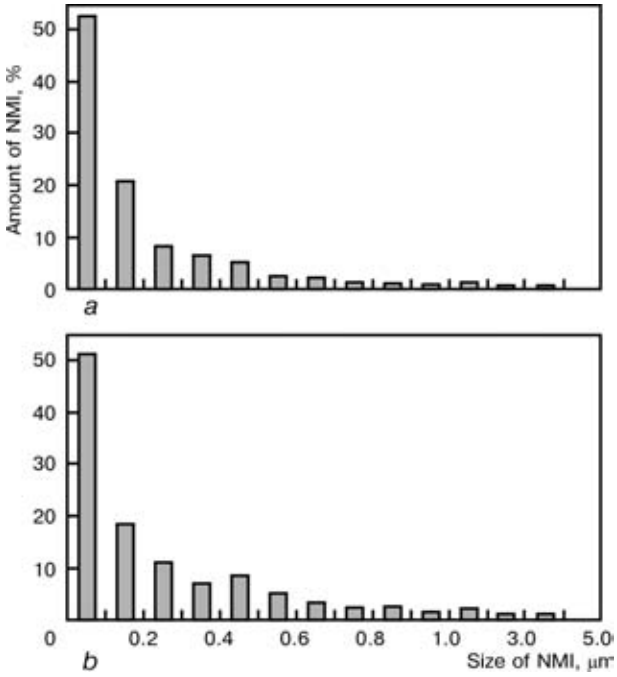

Figure 2. Distribution of NMI by sizes using SEM (*a*) and LM (*b*)

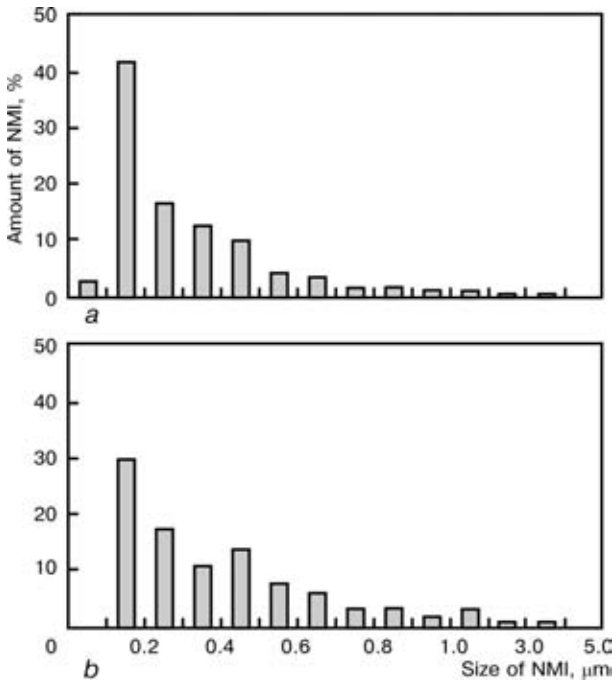

Figure 3. Distribution of NMI by sizes with allowance for removed noises: *a* — SEM; *b* — LM

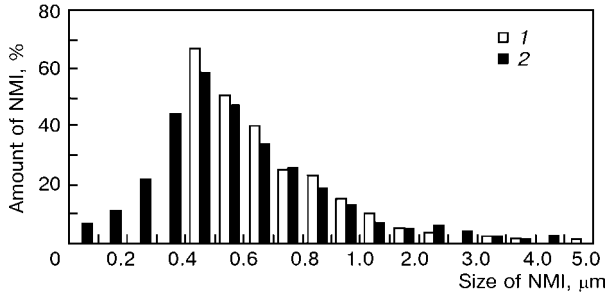

Figure 4. Histogram of NMI distribution, obtained using LM (*1*), equipped with a digital camera, and image analyzer «Omnimet» (*2*)

is directly associated with decrease in the area examined. The investigations showed that to obtain valid results it is necessary to analyze at least 250–300 fields. It was established in this case that the minimum size of particles to be determined is 0.022 μm.

It should be noted in conclusion that the comparison of histogram of NMI distribution, obtained using LM, equipped with a digital camera, and data, determined using «Omnimet» analyzer of images, showed their good enough correlation in the range of inclusion sizes of more than 0.5 μm (Figure 4) (samples are cut from another weld area). However, the volumetric share of NMI, obtained using a digital camera, is somewhat higher than the volumetric share of inclusions obtained by the automated method, i.e. 1.0 and 0.6 %, respectively. This is due to the fact that in calculation of inclusions by the image analyzer the inclusions of size of smaller than 0.5 μm are not determined. The application of the optical method of determination of NMI sizes using a digital camera will provide an opportunity to determine inclusions whose size exceeds 0.07 μm that is inaccessible at this stage for the metallographic method and automated systems for the image analysis.

Distribution of NMI amount in sizes

Size of inclusions, μm	*SEM*		*LM*	
	Amount, pcs	*%*	*Amount, pcs*	*%*
0.0–0.1	17	2.982456	0	0
0.1–0.2	240	42.10526	88	29.93197
0.2–0.3	94	16.49123	52	17.68707
0.3–0.4	74	12.98246	32	10.88435
0.4–0.5	57	10.00000	41	13.94558
0.5–0.6	25	4.385965	23	7.823129
0.6–0.7	20	3.508772	18	6.122449
0.7–0.8	11	1.929825	10	3.401361
0.8–0.9	10	1.754386	10	3.401361
0.9–1.0	7	1.228070	5	1.700680
1.0–2.0	9	1.578947	9	3.061224
2.0–3.0	3	0.526316	3	1.020408
3.0–4.0	3	0.526316	3	1.020408
4.0–5.0	0	0	0	0

Note. Averaged volumetric share of NMI in the field examined is 1.21 (SEM) and 1 % (LM).

It is possible to state on the basis od investigations that the value of a volumetric share and nature of distribution of NMI which sizes are smaller than 0.5 μm should be determined using SEM and LM, equipped with a digital camera. If a mean size of inclusions in the weld metal is smaller than 0.5 μm, then it is possible to use the traditional methods of NMI calculation.

The procedure developed can be used not only for NMI calculation, but also for determination of size and nature of distribution of any types of structural components in the weld metal.

PRECISION EXPLOSION WELDING OF STRUCTURES

L.D. DOBRUSHIN
E.O. Paton Electric Welding Institute, NASU, Kyiv, Ukraine

The concept of precision explosion welding based on the use of methods and techniques that minimise the pulse effect on a structure and its members is considered. New technologies and products made by these technologies are described, showing the capabilities of precision explosion welding in terms of solving various problems of modern welding production, which are difficult or impossible to solve by other welding methods.

Key words: *precision explosion welding, structures, structural members, tubular adapters, target cathodes, aluminium and copper busbars, bimetal suspensions, electrolytic cells*

The explosion welding (EW) process is still finding a wide and, at the same time, rational application in modern welding production. The primary application of EW is to produce flat and tubular bimetal and/or multilayer billets and semifinished products from different combinations of dissimilar materials, followed, as a rule, by processing to make specific small-size parts [1, 2]. There are cases when it is necessary to solve problems associated with structural EW, where welding is performed on a finished structure and a resulting joint usually requires no further processing [3]. However, in the majority of cases solutions of such problems are limited because of excessive residual distortions accompanying the EW process (characterised by high pressures and pulses) or even failure of a structure in the welding and/or cladding zone.

The E.O. Paton Electric Welding Institute is developing the concept of precision explosion welding (PEW) of structures and their members, primarily on limited and/or long-length surfaces, using methods and techniques intended for minimising the pulse effect on a structure. They are based on optimisation of conditions of formation of a welded joint near the lower bound of the process, increase in energy intensity of the EW parameters and flow diagrams, and prevention of inadmissible residual distortions of a structure in the welding and/or cladding zone. Below we describe the new technologies and the resulting products, showing the capabilities of PEW in terms of solving various problems arising in modern welding production.

Cu + Ti tubular adapters for refrigerators. Combining welding operations with simultaneous forming (EWF) for explosion treatment of metals is one of the efficient ways of improving the rational utilisation of energy of an explosive. The publications available on this matter [4] provide basic information on peculiarities of realisation of the combined EWF process and describe the procedure for calculation of its main parameters, primarily for bimetal billets in the form of part of a cylinder or like that. In this article we consider results of investigation into the possibility of using this method for production of Cu + Ti tubular adapters of a variable section [5], meeting the following sufficiently stringent technical requirements:

- a copper tube 50 (dia.) × 2 mm and 50 mm long should be welded to a titanium tube 20 (dia.) × × 2 mm and 20 mm long;
- the joint between the copper and titanium tubes should be of an overlap type, the length of the overlap should be no more than 10 mm;
- the joint in the adapter should be resistant to heat during subsequent arc welding, and should withstand the test pressure of up to 1.5 MPa.

Based on the above technical requirements, the task posed was to develop such a precision EWF technology, with which the energy of a precisely weighted (miniature) explosion charge would be distributed in succession and, at the same time, continuously for welding the titanium and copper tubes and forming (expanding) of the latter in a die to form the required final configuration of the adapter. As shown by preliminary experiments, there is no way of expanding the copper tube with an almost 2.5-fold increase in the outside diameter by avoiding fracture of the tube wall. The positive results were obtained through preliminary mechanical forming of the copper tube with a certain expanding cone and subsequent explosion forming using the inside rod-shaped explosive charge and water as a transmitting medium.

The angular diagram of the EW process was employed for overlap joining of the tubes in a very short region (no more than 10 mm) simultaneously with the explosion forming process. For this, a cone groove was made in the copper tube to form an angular gap between the mating surfaces of the tubes. Allowing for this fact, as well as for thinning of the copper tube during forming, thickness of its wall was increased to 3 mm. Basic geometrical parameters of the overlap with a cone groove and value of the angle of the cone for preliminary expanding of the copper tube were determined by the calculation-experimental method. Appearance of the resulting welded-formed adapter is shown in Figure 1.

The joining zone of the copper and titanium tubes was examined by metallography and ultrasonic inspection. At an initial width of the angular gap (groove) equal to about 10 mm the width of the joining zone was found to range from 7 to 8 mm, its mean surface area being $S_w \approx 5$ cm^2. The calculated weight

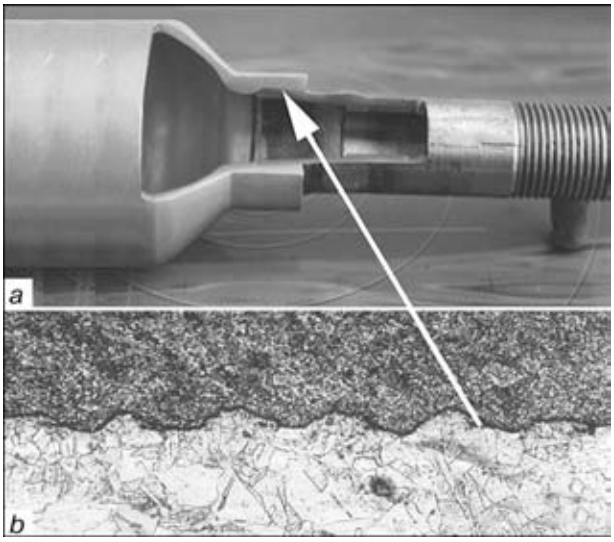

Figure 1. Macrosection of the Cu + Ti tubular adapter of a variable section (*a*) and microstructure of the joining zone (*b*) (×156)

of the explosive being equal to m_e = 2.1 g, its specific consumption was η_c = 0.42 g/cm^2 (weight of the explosive consumed for initiation of the rod-shaped explosive charge was ignored in the calculation). This is several times as low as in conventional EW and evidences a sufficiently high efficiency of the precision EWF technology developed. As seen from Figure 1, the interface of the joint has a regular wavy profile and contains no defects, including no thermomechanically affected regions which often accompany the process of the EW joint formation.

Temperature fields formed during subsequent argon-arc welding of the adapter to the above copper and titanium tubes were measured. It was found that the maximum temperature of the joining zone during subsequent arc welding did not increase to above 350 °C, and the time of heating it to this temperature did not exceed 6–7 min. Metallography revealed no negative effect of postweld heating on the quality of the resulting Ci + Ti joint. Reliability of the examination results was proved by successful tests of the adapters to internal pressure of up to 1.5 MPa.

An experimental batch of the adapters thus made was transferred to the Customer from the Republic of Korea for further tests under industrial conditions to be applied at refrigerators.

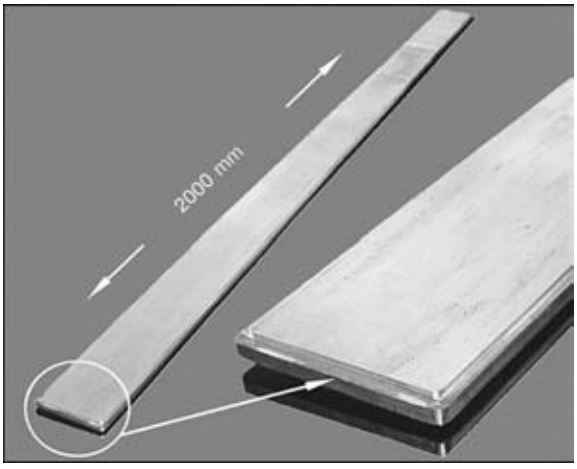

Figure 2. Long Cu + Ag bimetal target cathode produced by the precision explosion welding technology

Cu + Ag target cathodes for spraying of glass. The main cause of unsatisfactory heat insulation of window glasses consists in their ability to transmit not only visible solar radiation, but also invisible infrared one. To impart the properties of a filter hindering infrared radiation to the window glass, a thin layer of metal, e.g. silver, which reflects this radiation is deposited on the glass surface. Deposition of metals or semiconductors on glasses is done by magnetron sputtering in a vacuum chamber. To realise the sputtering process, it is necessary to use special target cathodes based on the Cu + Ag bimetal, in which the copper substrate serves as a cooler and the cladding silver layer serves for sputtering in the chamber.

The Cu + Ag bimetal target cathodes of the magnetron have the form of a strip about 2 m long and 100 mm wide. Thickness of the cladding silver layer ranges from 4 to 5 mm, whereas thickness of the copper substrate is not less than 10 mm. EW is in fact the only process available for the manufacture of this type of the bimetal target cathodes. Studies were conducted and the technology was developed for long narrow-strip explosion cladding of the copper substrate with the silver layer (both materials being of a commercial purity). The tasks of the studies included finding a solution to such problems as ensuring a high reliability of the process of detonation of a long explosive charge, elimination of lack of fusion on the perimeter of the cladding layer and prevention of residual distortions (deflections) of a part after cladding. Figure 2 shows the bimetal target cathode about 2 m long produced by the developed PEW technology. The target is photographed on a glass with a silver coating 14 nm thick deposited by using this target.

The PEW technology can be employed to manufacture similar target cathodes based on the Cu + Sn and Cu + Ti bimetals, as well as other combinations of metals and alloys.

The sprayed glasses are manufactured by Company «Tekhnoluch» at PWI.

Cu + Al anode busbars for electrolytic cells. There are such designs of different-application electrolytic cells which require joining of flexible multilayer aluminium bus ducts to a monolithic anode copper busbar by ensuring a reliable joint and an electric contact (both materials being of a commercial purity). EW is the most efficient and quality process of all other available methods used to join aluminium to copper. At the same time, this problem involves more difficulties than EW of monolithic aluminium and copper busbars. It was solved by using a combined method of joining the above current-conducting elements, as shown in Figure 3.

Two narrow aluminium strips 25 × 5 mm (Figure 3, *a*) were explosion welded to the copper busbar 275 × × 130 × 16 mm on both sides along its width (130 mm) at a distance of 37 mm from the lower end. Two

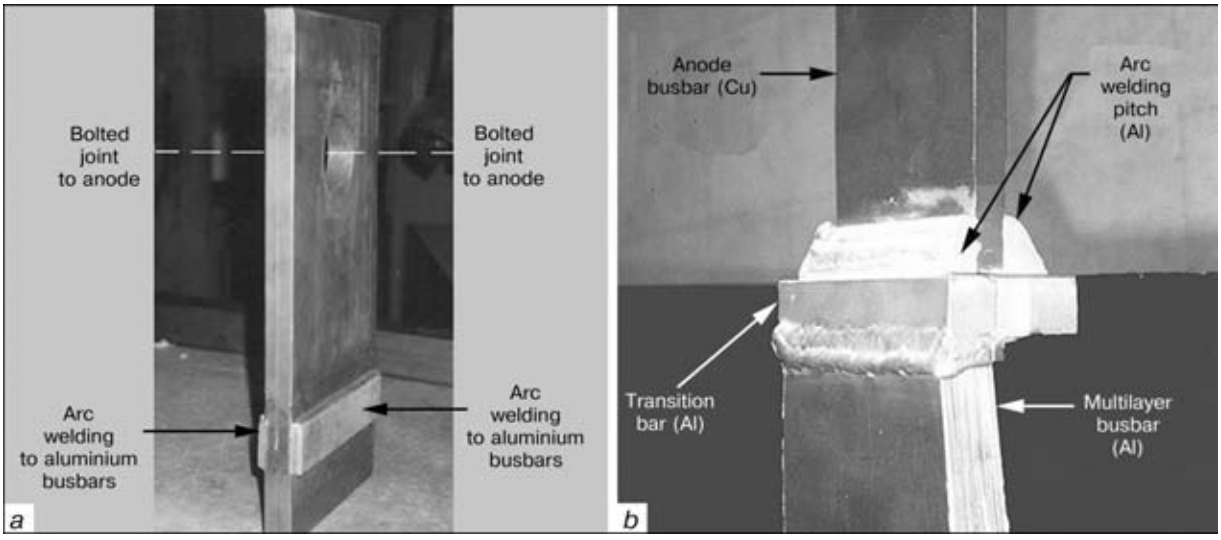

Figure 3. Appearance of the copper busbar explosion clad on two sides with narrow aluminium strips (*a*), and appearance of a welded joint between the flexible aluminium busbar and the copper busbar (*b*)

aluminium transition bars 25 × 25 mm were joined to the strips. Then the bars were joined to the aluminium strips by fillet arc welding in several passes. After the copper busbar cooled down to room temperature, flexible multilayer stacks of aluminium bus ducts, consisting of 46 layers each 0.5 mm thick, were butt arc welded to the transition bars (Figure 3, *b*).

For optimisation of the PEW technology it was necessary to provide a local narrow-strip explosion cladding of the copper busbar by avoiding lack of lateral fusion. For this we developed a new technique based on the use of a special inertia device around the explosion charge. Almost absolute absence of the lack of lateral fusion cases and the possibility of reusing the inertia device were experimentally proved.

Long Cu + Al bimetal busbars. The next characteristic example of the efficient and almost no-alternative application of the PEW process is production of contact joints between aluminium and copper busbars. Bolted joints between such busbars have decreased electrical conductivity, which deteriorates with time because of oxidation of the contact surface of the aluminium busbar, especially during operation of the joints under the increased temperature conditions. To solve this problem, we developed the PEW technology performed under conditions of shutdown of the process of detonation of a flat explosive charge to explosion weld the ends of the long ($L \approx 2$ m) plate aluminium busburs to the copper plate busbars, having the same sections equal to 100 × 10 mm. To avoid the initial lack of fusion, the end region of the aluminium busbar is placed with overhanging about the copper plate to a length of about 50 mm, wherefrom the process of detonation of the explosive charge is initiated. After initiation, the detonation process is stopped (shut down) strictly at the edge of the copper busbar. As a result, this provides the high-quality welding of the busbars with no damage of the long aluminium busbar at the location of shutdown of the explosive charge detonation (Figure 4). The photo shows an approximate collision angle at the moment of shutdown of the detonation and a smooth bending shape of the welded end region.

The work described was performed by an order of the Research and Production Company «Ferolit» (Kremenchug) with a purpose to install and test the produced transition joints in current-conducting units of induction furnaces intended for production of synthetic cast iron from steel scrap. The full-scale tests of the resulting transition joints for more than a year of operation under a current load of 2500 A showed that they were never heated to above 30 °C. This evidences the absence of considerable electrical resistance and voltage drop at the explosion welded interface between the long aluminium and the copper plate busbars.

Steel + Cu contact suspensions for electrolytic cells. The «Pankom-Yun» Company (Odessa) with participation of PWI has recently arranged the first Ukrainian production for electrolysis of super-pure cathode copper. For that it was necessary to develop the technology for PEW of bimetal contact suspensions, consisting of stainless steel plate 300 × 110 × × 3 mm clad in the centre with the copper plate 110 × × 100 × 1.5 mm. The clad plate is bent by the cladding layer inward to produce the П-shaped profile

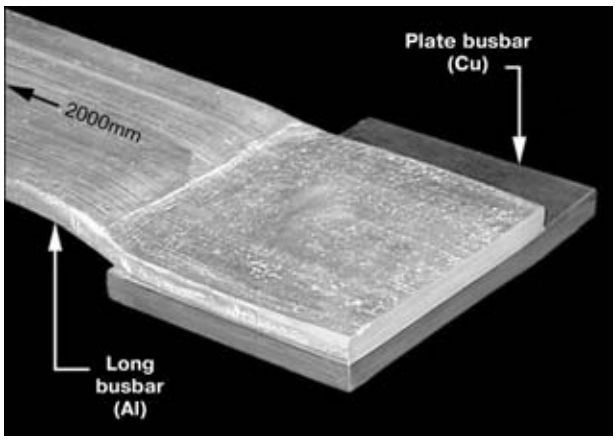

Figure 4. Transition welded joint between the long (L = 2 m) aluminium busbar and the copper plate busbar

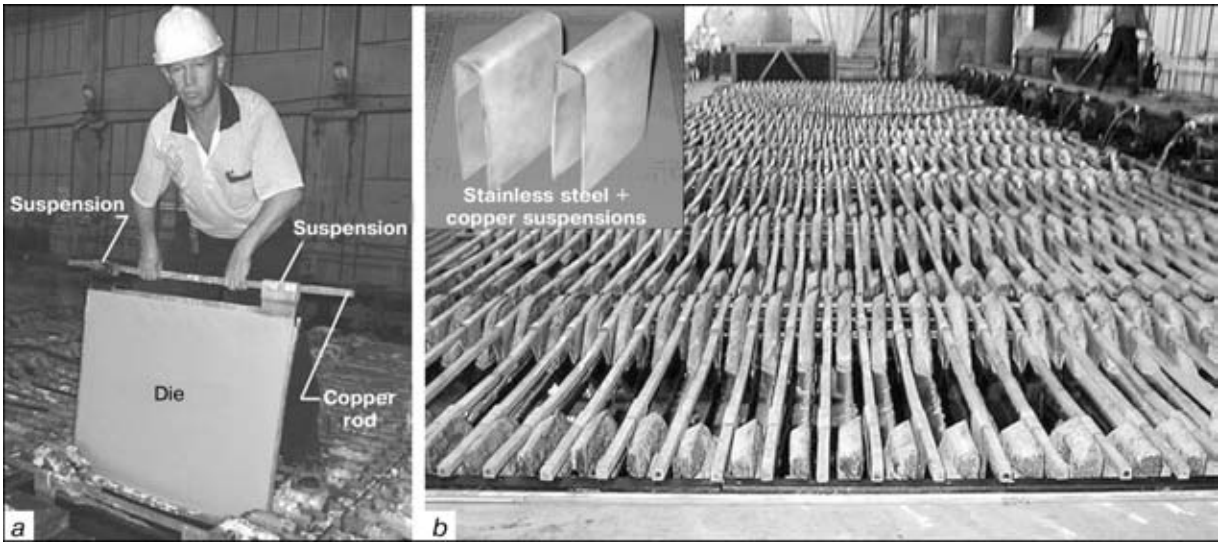

Figure 5. Types of dies with contact suspensions explosion clad with the copper layer in the zone of contact with the copper rod busbar (*a*), and cathode copper electrolysis workshop (*b*)

(Figure 5, *b*). The suspensions are fusion welded to the stainless steel die measuring 1600 × 900 × 3 mm. Then, by passing through the suspensions the copper rod busbar with a section of 22 × 22 mm (Figure 5, *a*), the die suspended to the copper rod busbar is lowered into the electrolytic bath (Figure 5, *b*). The presence of the cladding copper layer on the suspensions provides a reliable electric contact between the copper rod busbar and the die on which pure copper is deposited.

Production of a strong and electrically conducting joint between copper and stainless steel by the EW process hardly involves any difficulties. However, in this case it was necessary to develop the technology for mass production of the suspensions by avoiding distortion of the latter and lack of fusion at the edges. For this we developed the so-called cassette technology of explosion cladding. This technology allows from 5 to 10 bimetal billets of the suspensions to be produced per detonation. The total number of the suspensions which can be produced during a working day is up to 200 pieces. The experience of more than 2 years of operation of the suspensions, the operation conditions being unfavourable for the electric contact joints because of the effect of electrolyte vapours, showed that the zone of their contact with the copper rod busbar was never heated to above 40–50 °C, which is acceptable. The future plans are to use titanium dies and, hence, produce suspensions based on Ti + Cu bimetal.

Therefore, the described technologies and the resulting products show new capabilities of PEW in terms of solving various problems of welding production.

1. Kudinov, V.M., Koroteev, A.Ya. (1978) *Explosion welding in metallurgy*. Moscow: Metallurgiya.
2. Konon, Yu.A., Pervukhin, L.B., Chudnovsky, A.D. (1987) *Explosion welding*. Ed. by V.M. Kudinov. Moscow: Mashinostroenie.
3. Kobelev, A.G., Lysak, V.I., Chernyshev, V.N. et al. (2002) *Production of metallic laminated composite materials*. Moscow: Intermet Engineering.
4. Kuzmin, V.I., Lozovskaya, V.F., Gurikov, V.M. (1985) Peculiarities of explosion welding process with simultaneous forming. In: *Explosion welding and properties of welded joints*. Volgograd: VPI.
5. Dobrushin, L.D., Bugaets, V.P. (1998) Production of «copper-titanium» tubular adapters of a variable section using the method of precision explosion welding with simultaneous forming. In: *Proc. of Int. Conf. on Laminated Composite Materials*, Volgograd, Sept. 1988. Volgograd: VolgGTU.

ENSURING ENVIRONMENTAL AND OPERATIONAL SAFETY OF WELDING PRODUCTION IN RUSSIAN SHIPBUILDING*

V.D. GORBACH[1] and **V.V. CHERNYKH**[2]
[1]FGUP «TsNIITS», St.-Petersburg, Russia
[2]Russian Research and Development Welding Society, Moscow, Russia

Considered are the systems ensuring environmental and operational safety of welding production in shipbuilding and their harmonisation with international standards.

Key words: *welding production, shipbuilding, ecology, safety, examination, standards*

The scope of application of welding in many countries throughout the world is determined by a technological level of production as a whole. Wide spectrum of welding technologies, their non-waste character and, first of all, availability provided a high demand for and high volume of utilisation of welding in shipbuilding, where the labour input of welding operations amounts to 30–40 % of the total labour input in fabrication of ship hulls.

Substantial improvement in quality of welding operations and increase in operational and environmental safety of welding and welding-assembly productions are now the most important goals of the industry. These goals are planned to be achieved through implementation of a package of organisational-technical arrangements to ensure transition to a new, internationally harmonised level of training of the staff involved in welding production, ensuring independence and objectiveness of its certification, and mandatory fulfilment of requirements to operational and environmental qualification of the welding technology.

Shipbuilding is one of the industries where environmental and operational safety is a very topical issue. Welding production here is characterised by the most unfavourable labour conditions. The job of a welder is still one of the most hazardous, and the processes of welding, surfacing and cutting of metals are traditionally the focus of attention of the environment and labour protection specialists. A combined affect on welders by harmful industrial factors (Table), such as chemical (welding fumes, gases), physical (arc radiation, electromagnetic fields, physical and heat loads etc.) and natural ones, leads to development of occupational diseases and reduction in duration of their employment. Improvement of welding processes leads to decrease in utilisation of welding consumables and reduction of pollutant emissions into the atmosphere.

The Russian shipbuilding uses a system for development of technical and organisational solutions to ensure labour safety and environment protection in the manufacture of shipbuilding products, including in performing welding and cutting processes (Figure 1). An active role in this field is played by Federal State Unified Enterprise «Central Research Institute for Shipbuilding Technologies» (FGUP «TsNIITS»), which for more than 30 years has been the head organisation in the industry in charge of operational safety, and since 2000 also in charge of environment protection. During the previous years «TsNIITS» formed the scientific-and-technical potential for the above areas and trained qualified specialists.

This activity resulted in formation of the system for examination and sanitary-hygienic evaluation of processes, materials and equipment being developed. The experimental sanitary-hygienic investigations of processes and materials are conducted, if necessary. The certified sanitary-chemical laboratory was founded for this purpose within the «Gosstandart» (State Standard) system.

The databank on harmful emissions during the basic technological processes employed in the industry was generated on the basis of examination of the processes, materials and equipment developed. Regulatory documents on ensuring the operational safety in welding and cutting of aluminium-magnesium and titanium alloys performed in closed premises using mechanised production lines were developed and introduced into the industry with participation of «TsNIITS». Ventilation systems built into the welding equipment, as well as industrial ventilation systems applied at the industry enterprises are being designed and developed on the basis of the «TsNIITS» documents.

Advances in ensuring operational safety at the industry enterprises under the new economic conditions led to foundation of the Training Centre «Rhythm-Labour Protection» in 1999, incorporated into the Institute. In February 2001 the Ministry of Labour

* Information given in this article was presented at the International Conference on Protection of Environment, Health and Safety in Welding Production, Odessa, Ukraine, Sept. 11–13, 2002.

Labour conditions in performing welding operations in shipbuilding

Type of production	*Working zone air*	*Microclimate*	*Illumination level*	*Noise and vibrations*	*Non-ionising radiation*
Hull processing	Dust of metal oxides and scale are at a MAC level Gases (nitrogen oxides, CO) are from 1.5 to 7 of MAC Fumes, paintwork materials, vapours of solvents are at the MAC level	Lower than MAL in cold seasons, normal in warm seasons	Lower than MAL in building up, marking and welding sections	Noise is higher than MAL by 8–11 dB (A)	UV radiation is higher than MAL hundreds of times, IR radiation is higher than MAL by a factor of 3–4
	Welding fumes are higher than MAC by a factor of 5 to 19, manganese oxides are higher than MAC by a factor of 3 to 26, abrasive dust is higher than MAC by a factor of up to 30	Same	Lower than MAL in marking and welding sections	Noise is higher than MAL by 5–17 dB (A) Vibrations are higher than MAL at chippers and stripping machines	UV radiation during welding is higher than MAL hundreds of times, IR radiation is higher than MAL at currents above 300 A
Jig-based hull construction	Welding fumes during welding in closed rooms are higher than MAC by a factor of up to 20, manganese oxides are higher than MAC by a factor of up to 30	Lower than MAL in cold seasons in ship houses, higher than MAL in warm seasons at open slipways	Lower than MAL in closed and hard-to-reach locations	Noise is higher than MAL by 7–17 dB (A) Vibrations are higher than MAL by 2–8 dB (A)	Same

Notes. Here MAC — maximum admissible concentration, MAL — maximum admissible level, UV — ultraviolet and IR — infrared radiation.

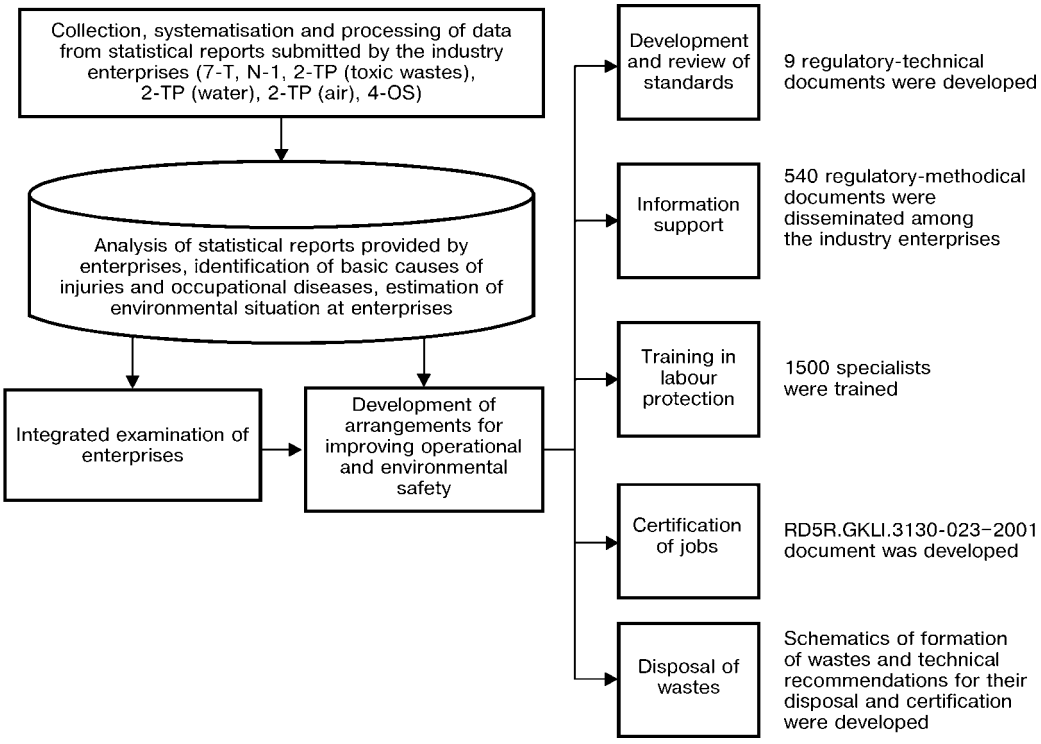

Figure 1. Block diagram of pursuing the state policy in the field of operational and environmental safety in shipbuilding (2001)

gave the permission for the Centre to provide training in operational safety, which allowed the studies to be performed not only in the north-western part, but also in other regions of the country. The teaching staff of the Training Centre consists of the skilled specialists from the operational and environmental safety laboratory certified for the teaching activity. More than 1500 people have been trained since the foundation of the Centre.

Certification of welding technologies was arranged, in addition to training and certification of the staff involved in welding production. The required production and research facilities fitted with means and methods for inspection of the quality of welded joints, as well as the properly trained specialists certified in compliance with the established procedure, allowed the «Independent Body for Non-Destructive Testing» to be accredited at «TsNIITS».

The operational and environmental safety of welding production in the industry is favoured by the concentration of diverse, methodically interrelated educational services, examination of safety of potentially hazardous enterprises and objects, design and manufacture of new welding equipment and introduction of the inspection means and methods at «TsNIITS».

Changes taking place nowadays in Russia apply, in particular, to the character of interaction between manufacturers, suppliers and customers. Trying to attract attention of a customer to his products, establish long-term contacts, and participate in bids to receive state and other orders, the Russian manufacturer expresses an increasingly high interest in development and application of the quality and environmental safety management systems, as well as in maintaining them at a proper level. «TsNIITS» has a certificate for the quality system, stating that it meets requirements of the relevant international standards.

Many enterprises, companies and even whole countries tend to refuse from interaction with partners who have no certificate for fitness to ISO 14000. Environment protection is becoming the important part of competition in domestic and especially international markets. Introduction and certification of the environment management system help to maintain the reputation of a company and achieve the main target, i.e. decrease the negative effect on the natural environment, in addition to providing other benefits to the company.

To be successfully integrated into the world exchange of commodities, it is necessary to increase competitiveness of industrial products and, therefore, turn to international and European standards in the field of welding in such areas as welding consumables and equipment, welding technologies, personnel, testing methods, ecology etc.

Topicality of the problem of environment protection and recovery is so apparent that governments of the EU countries, together with managers of industrial companies, have come to a conclusion of the necessity of foundation of the system to monitor condition of the environment, based on unified conceptual approaches and practical EU standards. This system should take a full account of peculiarities and specific features of a national legislation of each country in the field of the natural environment protection and recovery.

On this basis, the policy in welding production should be governed by the principles of introduction of the national versions of international standards ISO and European codes EN.

The environment monitoring system (EMS), based on the ISO 14000 series standard, is shown in Figure 2.

Realisation of a package of organisational-technical arrangements associated with education, training and certification of welders and welding production specialists at specialised centres, industrial and research certification of welding technologies, as well

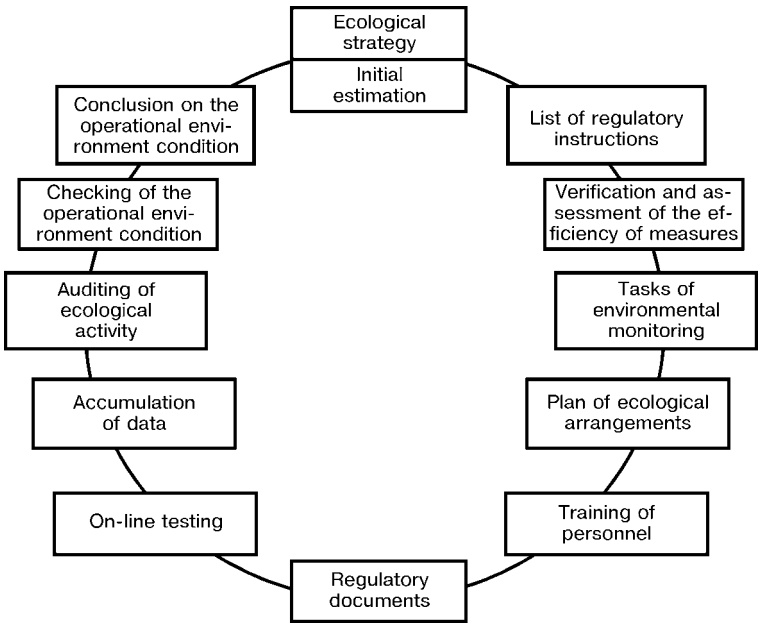

Figure 2. Environment monitoring system according to ISO 14000

as exchange of experience and holding of conferences, will provide an efficient handling of the problems of ensuring operational and environmental safety of welding production. This will require the following measures to be taken:

- development, utilisation and improvement of regulatory requirements specifying activity in the sphere of ecology;
- identification of the priority issues for handling the consequences of business activity of an enterprise having a negative effect on the environment, identification of the chief points of the negative effect of each object of an infrastructure;
- development of a package of measures to eliminate the negative effect on the environment, proceeding from the initial estimation of its condition and requirements of a national legislation. For this, it is necessary that the planned measures be by all means agreed upon with controlling bodies and organisations;
- identification of specific targets and tasks for the environment protection and recovery on the basis of the approved policy;
- management of the system of education and training of the staff intended for realisation of the specific tasks associated with ensuring environmental monitoring (EM);
- development of a set of governing documents, instructions and regulations for each type of business activity;
- identification of the order of controlling fulfilment of the requirements specified in the above documents and monitoring of practical activity in the sphere of ecology;
- continuous record keeping on the EM results;
- systematic evaluation of the effectiveness of EMS, its adequacy to requirements of specific conditions for improvement of the environment, and sensitivity to consistent upgrading of practical actions in this area;
- preparation of regular and well-grounded information on the environment condition and constant updating of databases on this problem.

The quality management systems (ISO 9000) have been applied and are successfully functioning at many Russian enterprises. Being organically integrated into the quality management systems for products and services existing at an enterprise, the environment management system favours improvement of ecological compatibility of products and production, and enables the activity of an enterprise in the environment management field to be made cost effective.

At the same time, double certification under parallel sets of standards (series 9000 and 14000) does not only lead to organisational difficulties, but also requires extra funds. Strong premises exist today for development of international standards to cover also the other aspects of business activity of an enterprise, including labour protection and occupational health of the personnel. This has been already partially covered by standards ISO 9001–2000. Such aspects might increase in number in the future.

In our opinion, development and industrial application of the integrated quality management system, meeting requirements of standards of both series 9000 and series 14000, having a unified administration structure consisting of a package of means intended for planning, document management, inspection, analysis, process control and impact on the environment by production, and targeted at improvement of the quality of products, competitiveness and decrease in the negative effect on the environment by the activity of enterprises, are the most topical and pressing problems.

Based on the potential available, FGUP «TsNIITS» could implement the above arrangements in collaboration with the Russian Research and Development Welding Society and using experience and recommendations the International Institute of Welding and the European Welding Federation.

NOMOGRAM FOR DETERMINATION OF THE MODE OF CONSUMABLE ELECTRODE ARC WELDING IN A MIXTURE OF Ar + 25 % CO_2

JI CHENG CHUN and **I.F. KORINETS**
NTUU «Kyiv Polytechnic Institute», Kyiv, Ukraine

Deterministic-statistical mathematical model of weld shape was the basis to develop a nomogram, which allows determination of basic parameters of arc welding in a mixture of Ar + 25 % CO_2 of a square-butt joint by the specified dimensions of the weld (penetration depth, reinforcement height and weld width), taking into account the size of the gap in the butt, optimization of the mode by weld dimensions or, vise versa, determination of weld dimensions with the known welding mode.

Key words: *arc welding, Ar + 25 % CO_2 mixture, consumable electrode, butt joint, gap, welding mode, nomogram, optimization of weld dimensions*

Arc welding in CO_2 and in a mixture of Ar + 25 % CO_2 is widely accepted in fabrication of structures of low-carbon and low-alloyed steels. This method is used in the form of a mechanized process (welding with semi-automatic and automatic machines) and an automatic process (robotic welding). Calculation method for welding mode determination (based on a mathematical model of weld shape), unlike the tabular method, allows not only a sufficiently accurate determination of the mode parameters but also their optimization. Having a model, the calculation and optimization of the welding mode can be performed in a computer or graphically by a nomogram. The latter allows a visual, graphic and fast determination and optimization of the welding mode. It can be readily applied in slide-rules [1], directly in welding machines and in specialist training.

For several years the Chair of Welding Fabrication of NTUU «Kyiv Polytechnic Institute» has conducted research on mathematical simulation of weld shape in arc welding [2–4], which was the basis to develop nomograms and engineering methods of calculation and optimization of arc welding modes. A nomogram was proposed earlier [5], which allows these operations to be performed in consumable electrode CO_2 arc welding. It differs from the previous ones [6] by that not only penetration depth but also weld width (and, therefore, the coefficient of penetration shape) are used in it as the input parameter. However, weld convexity is absent, and the influence of the gap is taken into account approximately through the calculated penetration depth.

More perfect nomograms are proposed now, where the number of input geometrical parameters of the weld is increased. By these nomograms the welding mode can be determined taking into account penetration depth h, width of the weld e, of its convexity g, as well as the gap size in the butt b (Figure 1). As an illustration, a nomogram is proposed for determination of the modes of arc welding of a square-butt joint on low-carbon and low-alloyed steels in a mixture of Ar + 25 % CO_2 with Sv-08G2S wire of 1.2 mm diameter (Figure 2).

The nomogram consists of four parts. Its main part (Figure 2, *a*) allows determination of the main parameters (welding current and speed) in deposition of a bead ($b = 0$). If the gap $b > 0$, then we will first find the penetration depth in deposition by the size of the gap and assigned actual penetration depth (Figure 2, *b*). Then, by the same method the reinforcement height in deposition is found from the gap size and actual size of weld convexity (Figure 2, *c*), and these data are further used to find the sought parameters of the welding mode in the main part of the nomogram (Figure 2, *a*). The weld width under these conditions, which is not dependent on the gap size, is determined in the graph (Figure 2, *d*). As an illustration, with the assigned initial dimensions of the butt weld ($h = 3$ mm, $g = 1.5$ mm, $b = 1$ mm), the following main parameters of the welding mode were found from the nomogram: $I_w = 173$ A, $v_w = 9.9$ mm/s. Weld width was $e = 7.4$ mm.

This nomogram can be used to solve the inverse problem, i.e. determine weld dimensions by the as-

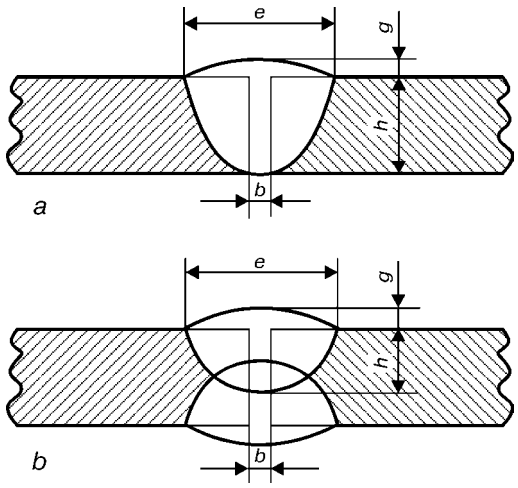

Figure 1. Dimensions of a weld in a square-butt welded joint: *a* — one-sided weld; *b* — two-sided weld

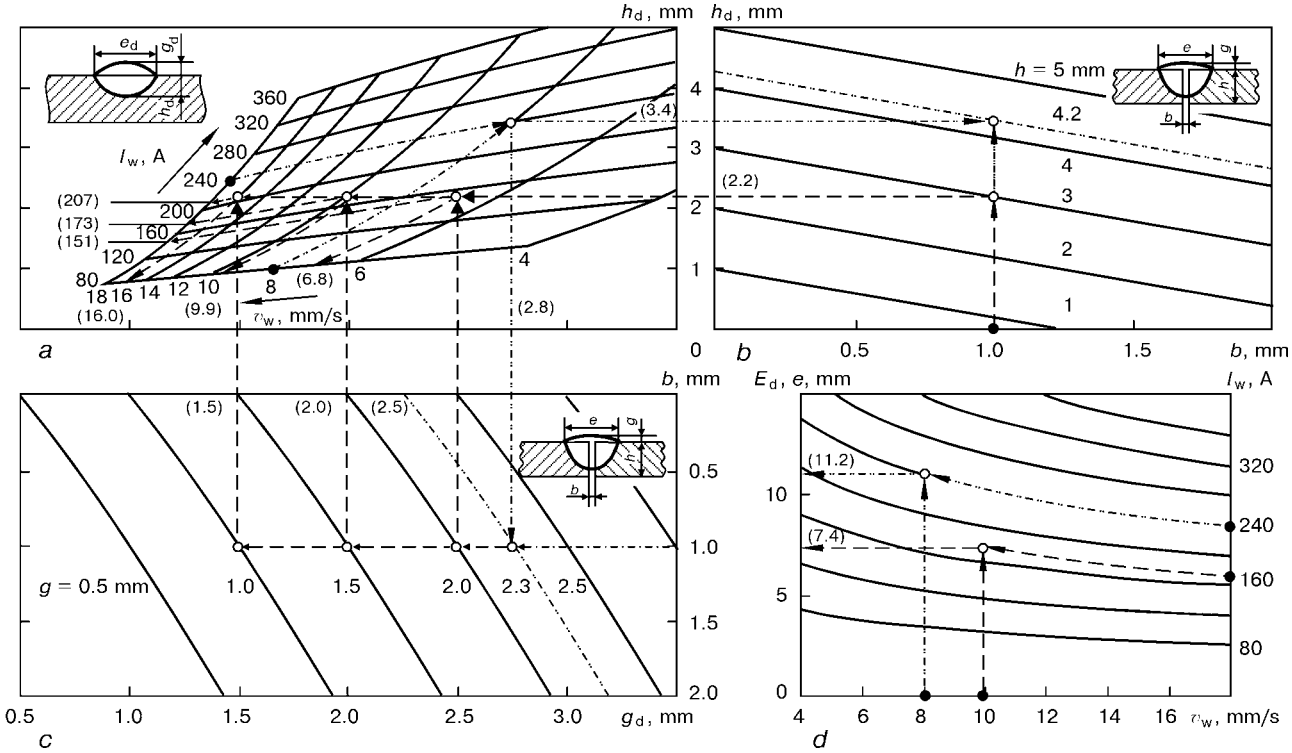

Figure 2. Nomogram for determination of the welding mode (hatched curve) and of weld dimensions (dash-dot curve) in MAG welding, taking into account the influence of the gap (for *a*–*d* see the text)

signed welding mode. For instance, the following mode is assigned: I_w = 240 A, v_w = 8 mm/s, b = = 1 mm. First in the main part of the nomogram (Figure 2, *a*) we will find the point of intersection of these parameters, and on the axes — the dimensions of the deposited bead (h_d = 3.4 mm and g_d = 2.8 mm). Then, we will allow for the influence of the gap on the penetration depth (Figure 2, *b*): at b = 1 mm we will find the actual penetration depth h = 4.2 mm and reinforcement height g = 2.3 mm (Figure 2, *c*). In Figure 2, *d* for I_w = 240 A and v_w = 8 mm/s, we find weld width to be e = 11.2 mm.

The nomogram allows optimization of the welding mode by its efficiency, which in single-pass welds is determined by the welding speed. In arc welding of low-carbon and low-alloyed steels, the thermal impact of the arc on the properties of the HAZ metal can be ignored. In this case the geometrical dimensions and weld shape can be taken as the criterion of the quality of a welded joint. During optimization of the welding mode the assigned penetration depth should remain constant, as it determines the penetration across the metal thickness. The height of weld reinforcement and its width can vary within the tolerance limit. Figure 2 shows an example of optimization of the welding mode at change of weld reinforcement. If it is increased from 1.5 up to 2 mm, then at a constant gap of 1 mm the welding current should be reduced from 173 to 151 A and the welding speed from 9.9 to 6.8 mm/s. In this case the weld width will become much smaller. Contrarily, if the weld convexity is reduced from 1.5 to 1 mm, it will be necessary to increase the welding current up to 207 A and the welding speed up to 16 mm/s. The weld width will be greatly increased. It is obvious that the second variant of the welding mode will be more efficient and cost-effective, as it provides a higher welding speed. The same optimization can be performed in this nomogram at the change of the weld width or gap size.

CONCLUSIONS

1. A nomogram has been developed to determine the main parameters of the mode of consumable electrode arc welding of low-carbon and low-alloyed steels in a mixture of Ar + 25 % CO_2 by weld dimensions and gap size, which differs from the existing ones by allowing for all the main geometrical parameters of a butt weld.

2. The nomogram can be used also to solve an inverse problem, namely determination of the dimensions of a weld by the specified mode of welding and size of the gap in the butt.

3. The nomogram allows optimization of the welding mode, for instance, by efficiency.

4. Nomograms of this type can be developed for optimization of welding heat input, deposited metal area, welding consumables consumption, power consumption and other criteria.

1. Sergatsky, G.I., Dubovetsky, S.V. (1981) Slide-rule for determination of CO_2 welding conditions. *Avtomatich. Svarka*, **4**, 41–43.
2. Korinets, I.F. (1988) Development of the engineering approaches of calculation of arc welding conditions. In: *Mathematical methods in welding*. Kyiv: PWI.
3. Korinets, I.F., Ji Cheng Chun (2001) Deterministic-statistical model of weld shape in arc welding. *The Paton Welding J.*, **10**, 39–44.
4. Korinets, I.F., Ji Cheng Chun (2002) Effect of gap on sizes of butt weld in consumable electrode arc welding in Ar + 25 % CO_2 mixture. *Ibid.*, **8**, 15–17.
5. Korinets, I.F., Okhaj, Yu.I. (1995) Nomograms for determination of CO_2 arc welding conditions. *Avtomatich. Svarka*, **10**, 46–48.
6. Shraerman, M.R. (1981) Nomograms for determination of parameters of submerged-arc welding of butt joints. *Svarochn. Proizvodstvo*, **8**, 17–20.

Developed at PWI

POWER SUPPLY FOR METAL-ELECTRODE PULSED-ARC WELDING

The possibility of smooth and independent regulation of parameters of pulses of the current in metal-electrode pulsed-arc welding (MEPAW) allows melting and transfer of electrode metal to be controlled in a desirable way, and physical-chemical and metallurgical processes occurring at the electrode and in the weld pool to be actively affected, thus providing the improved quality and increased productivity of the welding process. Existing power supplies IUP-1 and VDGI-302 have limited capabilities in terms of regulation of parameters of the pulses, especially in terms of their frequency. As a result, advantages of the MEPAW process are not utilised to a full degree.

Widening of application of MEPAW in engineering required development of a power supply with improved capabilities in terms of regulation characteristics.

Such a supply was developed by the E.O. Paton Electric Welding Institute. It allows the MEPAW process parameters, such as duration, amplitude and frequency of pulses of the welding current, as well as mean values of the current and arc voltage, to be smoothly and independently regulated. This provides easy and precise setting and regulation of the optimal welding conditions as required by a technology, which makes it possible to purposefully program the processes of melting and transfer of the electrode metal droplets at optimal values of their weight, diameter and temperature. Also, this leads to better composition, structure and properties of the weld metal and welded joints as a whole.

The possibility is provided for a programmed control of operation and parameters of the power supply by external programming units with a standard output from 0 to 10 V. This enables the power supply to be used in the synergic program control systems, such as those applied for position butt welding of pipelines and robotic complexes. Welding parameters are monitored by pointer-type instruments and digital light indicators, providing setting up of the parameters prior to welding and their control and regulation during welding.

Specifications of the power supply

Mains voltage, AC, 3-phase, 50 Hz, V	380
Mean welding current, A:	
minimum	50
maximum at duty cycle of 60 % and cycle time of 10 min	400
maximum at duty cycle of 100 %	315
Mean arc voltage, V:	
minimum	16
maximum	40
Pulse frequency smoothly regulated, Hz	30–300
Pulse duration smoothly regulated, s	$(1.5–5)\cdot10^{-3}$
Current pulse amplitude smoothly regulated, A	400–800
Welding wire diameters, mm:	
for welding aluminium, titanium and copper alloys	1.0–2.5
for welding steels	0.8–2.0
Overall dimensions, mm	850×630×1600
Weight, kg	not more than 400

Main applications include semi-automatic, automatic and robotic MEPAW of parts of aluminium-, titanium- and copper-base alloys in argon, helium and their mixtures, as well as low-carbon, low-, medium- and high-alloy steels in argon and Ar + CO_2 and Ar + CO_2 + O_2 mixtures. A widened range of smooth regulation of the process parameters allows utilisation of advantages of MEPAW in the manufacture of parts from different materials and in a large thickness range. Welding can be performed in any spatial position. Quality of welded joints meets requirements to the first category of the critical-application welds.

For more information please contact:
Tel.: (380 44) 227 44 78, 261 52 31